

11-2016

# Anomaly Detection Using Predictive Convolutional Long Short-Term Memory Units

Jefferson Ryan Medel  
jxm5998@rit.edu

Follow this and additional works at: <http://scholarworks.rit.edu/theses>

---

## Recommended Citation

Medel, Jefferson Ryan, "Anomaly Detection Using Predictive Convolutional Long Short-Term Memory Units" (2016). Thesis. Rochester Institute of Technology. Accessed from

# **Anomaly Detection Using Predictive Convolutional Long Short-Term Memory Units**

by

**Jefferson Ryan Medel**

A Thesis Submitted in Partial Fulfillment of the Requirements for the Degree of  
Master of Science in Computer Engineering

Supervised by

Dr. Andreas Savakis  
Department of Computer Engineering  
Kate Gleason College of Engineering  
Rochester Institute of Technology  
Rochester, NY  
November 2016

## **Approved By:**

---

Dr. Andreas Savakis

*Primary Advisor – R.I.T. Dept. of Computer Engineering*

---

Dr. Andres Kwasinski

*Secondary Advisor – R.I.T. Dept. of Computer Engineering*

---

Dr. Roy Melton

*Secondary Advisor – R.I.T. Dept. of Computer Engineering*

# **Dedication**

I would like to dedicate this thesis to my loving parents, Ric and Juliet Medel, and sister, Riane Medel, whom have given me unwavering support over the years.

# Acknowledgements

I would like to thank my advisor Dr. Andreas Savakis for his assistance and work guiding me through the development of this thesis, and my committee members Dr. Andres Kwasinski and Dr. Roy Melton for their time. I also want to thank my colleagues in the Computer Vision Lab, Peter Muller, Dan Chianucci, and Breton Minnehan, for their knowledge and company.

## Abstract

Automating the segmentation of anomalous activities within long video sequences is complicated by the ambiguity of how such events are defined. This thesis approaches the problem by learning generative models with which meaningful sequences can be identified in videos using limited supervision. We propose two types of end-to-end trainable Convolutional Long Short-Term Memory (Conv-LSTM) networks that are able to predict the subsequent video sequence from a given input. The first is an encoder-decoder based model that learns spatio-temporal features from stacked non-overlapping image patches, and the second is an autoencoder based model that utilizes max-pooling layers to learn an abstraction of the entire image. The networks learn to model “normal” activities from usual events. Regularity scores are derived from the reconstruction errors of a set of predictions with abnormal video sequences yielding lower regularity scores, as they diverge further from the actual sequence with time. The models utilize a composite structure and examine the effects of “conditioning” to learn more meaningful representations. The best model is chosen based on the reconstruction and prediction accuracies. The Conv-LSTM models are evaluated both qualitatively and quantitatively, demonstrating competitive results on multiple anomaly detection datasets. Conv-LSTM units are shown to provide competitive results for modeling and predicting learned events when compared to state-of-the-art methods.

## Table of Contents

Dedication .....	ii
Acknowledgements .....	iii
Abstract .....	iv
List of Figures .....	vii
List of Tables .....	xii
Glossary .....	xiii
Chapter 1 Introduction .....	1
1.1. Thesis Contributions .....	2
1.2. Thesis Outline .....	2
Chapter 2 Background.....	4
2.1. Feed Forward Neural Networks .....	4
2.2. Convolutional Neural Networks .....	5
2.3. Recurrent Neural Networks .....	7
2.3.1 Long Short-Term Memory .....	8
2.3.2 Convolutional Long Short-term Memory .....	10
2.4. Future Video Prediction.....	13
2.5. Anomaly Detection in Videos .....	17
Chapter 3 Anomaly Detection through Future Prediction .....	19
3.1. Proposed Architectures.....	19
3.1.1 Proposed Composite Convolutional LSTM Encoder-Decoder.....	19

3.1.2	Proposed Conv-LSTM Autoencoder.....	22
3.1.3	Parameters of Note .....	24
3.2.	Evaluation Algorithm .....	26
3.2.1	Parameters of Note .....	28
Chapter 4	Experimental Results.....	30
4.1.	Experimental Setup.....	30
4.1.1	Dataset Selection .....	31
4.2.	Preliminary Code Validation .....	34
4.3.	Parameter Selection .....	36
4.3.1	Model Parameters.....	36
4.3.2	Evaluation Parameters.....	38
4.4.	Results .....	39
4.4.1	Predicting Past and Future Video Sequences .....	39
4.4.2	Preliminary Anomaly Detection Evaluation .....	46
4.4.3	Improved Anomaly Detection Evaluation.....	46
Chapter 5	Conclusion .....	66
Bibliography	.....	68

## List of Figures

Figure 1: A Simple Feed Forward Neural Network. The nodes in the input layer is the input data, while the nodes in the hidden and output layers are perceptrons. Each connection between nodes represents a weighted connection. ....	4
Figure 2: Diagram illustrating the relationship between the input and layers. Each resulting feature map in the hidden layer uses its own convolutional filter. The filters process the input with a sliding window that sums the convolutional results across every channel at the same coordinate. ....	6
Figure 3: A visualization of the LeNet architecture. It combined convolutional, pooling, and fully connected layers to learn a model that can solve classification problems.....	7
Figure 4: Unrolled Recurrent Unit.....	8
Figure 5: Long Short-term Memory Cell.....	9
Figure 6: Inner Structure of a Conv-LSTM Unit .....	12
Figure 7: The composite structure for unrolled LSTM unit. Blue lines represent potential conditioning .....	14
Figure 8: Reconstruction and future prediction obtained from the Composite Model on a dataset of Bouncing MNIST images [19] .....	15
Figure 9: Reconstruction and future prediction obtained from the Composite Model on a dataset of natural image patches. [19] .....	16
Figure 10: Two prediction examples. All of the predictions and ground truths are sampled with an interval of 3. From top to bottom: input frames; ground truth frames; prediction by the ConvLSTM forecasting network. [17].....	17
Figure 11: High-level view of the Conditioned Composite Conv-LSTM Encoder-Decoder. The right side is the encoder, while the left is the decoder. The decoder is split into a present and future decoder, where the future decoder is potentially conditioned with the output of the current time-step feeding into the input of the next.....	20
Figure 12: High-level view of the Conditioned Conv-LSTM Autoencoder. The right side is the encoder, while the left is the decoder. The decoder uses an autoencoder format and is conditioned with the output of the current time-step feeding into the	

input of the next. The full composite model has a duplicate of the decoder with the target output being the input frames. ....	23
Figure 13: Three samples of the first ten frames from three sequences of the Bouncing MNIST dataset .....	31
Figure 14: Images from the UCSD Pedestrian dataset. The left and right columns are from the Pedestrian 1 and 2 subsets respectively.....	32
Figure 15: Images from the Subway dataset. The left and right columns are from the Exit and Entrance videos respectively.....	32
Figure 16: Images from the Avenue Dataset. ....	33
Figure 17: A comparison between prototype network outputs. Each column denotes a time-step sequentially from left to right starting at T+1. Each row from top to bottom represent the input sequence, the target ground truth future sequence, the forecasting model [17], the encoder-decoder prototype, and the autoencoder prototype. ....	35
Figure 18: Input reconstruction obtained from the Composite Conv-LSTM Autoencoder Model on a <i>non-anomalous</i> sequence from test clip 1 of the UCSD Pedestrian 1 dataset. The first row is the input ground truth video sequences, while the second is the input reconstruction. Each column denotes a time-step. Regions of interest that change through time are highlighted by a yellow bounding box.....	40
Figure 19: Future prediction obtained from the Composite Conv-LSTM Autoencoder Model on the <i>non-anomalous</i> sequence from test clip 1 of the UCSD Pedestrian 1 dataset used in Figure 18. The first row is the future ground truth video sequences, while the second is the output prediction. Each column denotes a time-step. Regions of interest that change through time are highlighted by a yellow bounding box.....	41
Figure 20: Input reconstruction obtained from the Composite Conv-LSTM Encoder-Decoder Model on a <i>non-anomalous</i> sequence from test clip 1 of the UCSD Pedestrian 1 dataset. The first row is the input ground truth video sequences, while the second is the input reconstruction. Each column denotes a time-step. Regions of interest that change through time are highlighted by a yellow bounding box.....	41
Figure 21: Future prediction obtained from the Composite Conv-LSTM Encoder-Decoder Model on the <i>non-anomalous</i> sequence from test clip 1 of the UCSD Pedestrian 1 dataset used in Figure 20. The first row is the future ground truth video sequences, while the second is the output prediction. Each column denotes a time-	

step. Regions of interest that change through time are highlighted by a yellow bounding box.....42

Figure 22: Input reconstruction obtained from the Composite Conv-LSTM Encoder-Decoder Model on an *anomalous* sequence from test clip 1 of the UCSD Pedestrian 1 dataset. The first row is the input ground truth video sequences, while the second is the input reconstruction. Each column denotes a time-step. Regions of interest that change through time are highlighted by a yellow bounding box.....43

Figure 23: Future prediction obtained from the Composite Conv-LSTM Encoder-Decoder Model on the *anomalous* sequence from test clip 1 of the UCSD Pedestrian 1 dataset used in Figure 22. The first row is the future ground truth video sequences, while the second is the output prediction. Each column denotes a time-step. Regions of interest that change through time are highlighted by a yellow bounding box.....43

Figure 24: Input reconstruction obtained from the Composite Conv-LSTM Encoder-Decoder Model on an *anomalous* sequence from test clip 29 of the UCSD Pedestrian 1 dataset. The first row is the input ground truth video sequences, while the second is the input reconstruction. Each column denotes a time-step. Regions of interest that change through time are highlighted by a yellow bounding box.....45

Figure 25: Future prediction obtained from the Composite Conv-LSTM Encoder-Decoder Model on the *anomalous* sequence from test clip 29 of the UCSD Pedestrian 1 dataset used in Figure 24. The first row is the future ground truth video sequences, while the second is the output prediction. Each column denotes a time-step. Regions of interest that change through time are highlighted by a yellow bounding box .....

45

Figure 26: A comparison between the original and improved model's regularity scores for testing clip 36 of the UCSD Pedestrian 1 dataset.....50

Figure 27: Regularity score (Eq.7) of test clip 29 of the UCSD Pedestrian 1 dataset. Distinct local minima are represented by a blue dot, distinct local maxima are represented by a red dot, the anomalous ground truth regions are highlighted in red, and the proposed anomalous regions are highlighted in green. ....50

Figure 28: Anomaly evaluation graphs of test clips from the UCSD Pedestrian 1 dataset. Smaller areas of interest are highlighted with a yellow bounding box.....51

Figure 29: Regularity score (Eq.7) of test clip #2 of the UCSD Pedestrian 2 dataset .....53

Figure 30: Anomaly evaluation graphs of test clips from the UCSD Pedestrian 1 dataset. Smaller areas of interest are highlighted with a yellow bounding box.....54

Figure 31: Input reconstruction obtained from the (224x224) Composite Conv-LSTM Encoder-Decoder Model on an *anomalous* sequence from test clip 1 of the UCSD Pedestrian 2 dataset. The first row is the input ground truth video sequences, while the second is the input reconstruction. Each column denotes a time-step. Regions of interest that change through time are highlighted by a yellow bounding box.....55

Figure 32: Future prediction obtained from the (224x224) Composite Conv-LSTM Encoder-Decoder Model on the *anomalous* sequence from test clip 1 of the UCSD Pedestrian 2 dataset used in Figure 32. The first row is the future ground truth video sequences, while the second is the output prediction. Each column denotes a time-step. Regions of interest that change through time are highlighted by a yellow bounding box .....55

Figure 33: Regularity score (Eq.7) of frames 40,000–60,000 of the subway entrance. Distinct local minima are represented by a blue dot, distinct local maxima are represented by a red dot, the anomalous ground truth regions are highlighted in red, and the proposed anomalous regions are highlighted in green. ....57

Figure 34: Regularity score (Eq.7) of frames 100,000-120,000 (top) and 120,000 – 144,000 (bottom) from the Subway Entrance video.....57

Figure 35: Input reconstruction obtained from the (224x224) Composite Conv-LSTM Encoder-Decoder Model on an *anomalous* sequence from the Subway Entrance video. The first row is the input ground truth video sequences, while the second is the input reconstruction. Each column denotes a time-step.....58

Figure 36: Future prediction obtained from the (224x224) Composite Conv-LSTM Encoder-Decoder Model on the *anomalous* sequence from the Subway Entrance video used in Figure 35. The first row is the future ground truth video sequences, while the second is the output prediction. Each column denotes a time-step.....58

Figure 37: Regularity score (Eq.7) of frames 37,500–52,500 of the subway exit video..60

Figure 38: Regularity score (Eq.7) of frames 7,500-22,500 (top) and 22,500 – 37,500 (bottom) from the Subway Entrance video.....60

Figure 39: Input reconstruction obtained from the (224x224) Composite Conv-LSTM Encoder-Decoder Model on an *anomalous* sequence from the Subway Exit video. The first row is the input ground truth video sequences, while the second is the input reconstruction. Each column denotes a time-step. Regions of interest that change through time are highlighted by a yellow bounding box.....61

Figure 40: Future prediction obtained from the (224x224) Composite Conv-LSTM Encoder-Decoder Model on the *anomalous* sequence from the Subway Exit video used in Figure 39. The first row is the future ground truth video sequences, while the second is the output prediction. Each column denotes a time-step. Regions of interest that change through time are highlighted by a yellow bounding box. ....61

Figure 41: Input reconstruction obtained from the (224x224) Composite Conv-LSTM Encoder-Decoder Model on an *anomalous* sequence from test clip 1 of the Avenue dataset. The first row is the input ground truth video sequences, while the second is the input reconstruction. Each column denotes a time-step. ....63

Figure 42: Future prediction obtained from the (224x224) Composite Conv-LSTM Encoder-Decoder Model on the *anomalous* sequence from the Avenue test clip used in Figure 41. The first row is the future ground truth video sequences, while the second is the output prediction. Each column denotes a time-step. ....63

Figure 43: Anomaly evaluation graphs of test sequences from the Avenue dataset. ....64

Figure 44: Regularity score (Eq.7) of test clip #1 of the Avenue dataset. ....65

## List of Tables

Table 1: A comparison of Loss between the prototype networks trained on the Bouncing MNIST dataset. ....	35
Table 2: Comparing reconstruction accuracy performance .....	37
Table 3: Comparing reconstruction accuracy performance .....	40
Table 4: Comparing anomaly detection performance of the proposed models on UCSD Pedestrian 1 dataset. There are a total of 40 anomalous events.....	47
Table 5: Average MSE per frame when evaluated on 64x64 pixel images using the specified parameters.....	48
Table 6: Comparing abnormal event detection performance across multiple datasets. Ours is the Composite Conv-LSTM Encoder-Decoder (64x64) model. * Improved ground truth on Subway Exit dataset. # Uses older dataset. ....	49

## Glossary

<b>LSTM</b>	Long Short-Term Memory
<b>Conv-LSTM</b>	Convolutional Long Short-Term Memory
<b>FC-LSTM</b>	Fully Connected Long Short-Term Memory
<b>CNN</b>	Convolutional Neural Network
<b>RNN</b>	Recurrent Neural Network
<b>MSE</b>	Mean Squared Error
<b>FC-LSTM</b>	Fully Connected Long Short-Term Memory
<b>ReLU</b>	Rectified Linear Unit
<b>TP</b>	True Positive
<b>FP</b>	False Positive

# **Chapter 1    Introduction**

Anomalies in videos are broadly defined as events that are unusual and signify irregular behavior. Detecting such irregularities is important, as errors and bugs must first be found before they can be addressed. Consequently, anomaly detection is an extensive field that can be applied in many different areas. One such area is in computer vision detecting irregular activities of interest in videos and can be applied to many real-world scenarios including surveillance and security.

Meaningful events that are of interest in long video sequences, such as surveillance footage, often have an extremely low probability of occurring. As such, manually detecting such events, or anomalies, is a very meticulous job that often requires more manpower than is generally available. This has prompted the need for automated detection and segmentation of sequences of interest [1]-[15].

In contrast to the related field of action recognition where events of interest that are clearly defined, anomalies in videos are often vaguely defined and may cover a wide range of activities. Since it is less clear-cut, models that can be trained using little to no supervision, including spatio-temporal features, dictionary learning and autoencoders [15] are more applicable to the problem of evaluating anomalies. The methodologies used by [1]-[15] were developed to detect anomalies within video sequences specifically and are effective in doing so. A description of these methodologies and their limitations are discussed in Section 2.5.

## **1.1. Thesis Contributions**

This thesis aims to make two main contributions. The first is the development of a model architecture able to encode an input video sequence, reconstruct it, and predict the subsequent sequence. Two such networks are proposed, an encoder-decoder and an autoencoder based model. The model utilizes Convolutional Long Short-Term Memory (Conv-LSTM) units that allow the neural network to better learn spatio-temporal features. Conv-LSTM units merge convolutional operations into traditional fully connected LSTM (FC-LSTM) units, and are further discussed in Section 2.3.2. The second is the ability to detect anomalous video segments through the model's output using a regularity evaluation algorithm. The regularity of a video sequence is relative to other sequences of the same source. A preliminary investigation on the validity of the network architectures using simplified versions are evaluated on the Bouncing MNIST dataset. The proposed networks are then evaluated on the UCSD Pedestrian 1 dataset. The best model is improved upon and further evaluated on the UCSD Pedestrian 2 dataset, Subway dataset, and Avenue dataset.

## **1.2. Thesis Outline**

This document is organized as follows: Chapter 2 discusses the prior work relative to the thesis domain and its influence on the proposed design. Chapter 3 discusses the proposed architectures, their various implementations, and the evaluation algorithm. The proposed architectures include a Conv-LSTM Autoencoder and a Conv-LSTM Encoder-Decoder model. Chapter 4 details the experiments of the proposed systems as well as their

results on various datasets. Chapter 5 provides a conclusion summarizing the potential and effectiveness of our system.

## Chapter 2 Background

### 2.1. Feed Forward Neural Networks

The Artificial Neural Network was first proposed by Rosenblatt in 1958 [32]. Neural networks are a biologically inspired model simulating the way a brain works. It connects multiple “neurons,” such that each individual neuron performs simple functions that include a nonlinearity, to model more complex tasks. A typical feed forward neural network consists of an input layer, output layer, and one or more hidden layers (Figure 1). The hidden and output layers are made up of perceptrons that weight their input connections and only activate when the values used within the unit’s function exceed a given threshold value. Every perceptron’s weights are updated through a backpropagation algorithm that aims to minimize the error between network output and target value.

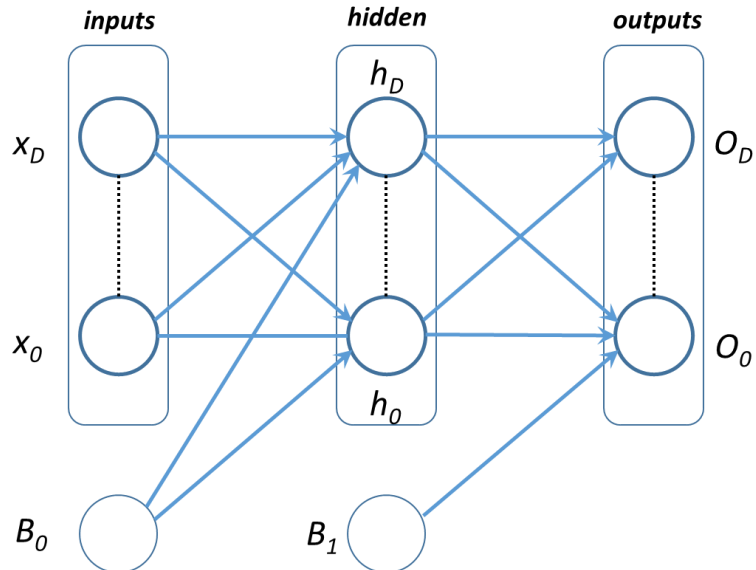


Figure 1: A Simple Feed Forward Neural Network. The nodes in the input layer is the input data, while the nodes in the hidden and output layers are perceptrons. Each connection between nodes represents a weighted connection.

Since the network learns its own weights, it is able to determine on its own what features are important and applicable to the task. While a strong tool, feed forward neural networks utilizing only perceptrons are not as effective on problems that rely on spatial or temporal information. This weakness has led to the development of Convolutional and Recurrent Neural Networks [39].

## 2.2. ***Convolutional Neural Networks***

Images and videos of similar articles are subject to inconsistency in properties that include translation, rotation and scaling. As such, invariance to transformations is a desirable property in any neural network dealing with vision. Invariance can generally be introduced into models in three ways: pre-processing the data to be invariant so any subsequent manipulation of the data will remain invariant, use regularization techniques like tangent propagation to penalize transformed data, and building the invariance properties into the network's structure [21]. The Convolutional Neural Network (CNN) initially proposed by LeCun [22], uses the third approach.

Convolutional Neural Networks (Figure 2) utilize three mechanisms: local receptive fields, weight sharing, and subsampling. The local receptive fields are organized into a plane called a feature map, with every field sharing the same weight. Each field captures local patterns within an image by connecting each neuron only to small regions of the input. This takes advantage of the fact that pixels that are close to one another are more strongly correlated than pixels that are far apart. Since the local receptive fields share the same weight, the evaluation of activation for each neuron is equivalent to the convolution

of the weight kernel with the sampled region of image pixel intensities. The neurons making up a plane are known as the convolutional layer. Sliding the local receptive field across the entire image allows features to be found regardless of position.

As the weights of a local receptive field are the same for each neuron in the convolutional layer, it can be seen that the convolutional layer is just an image *convolution* of the previous layer. The weights are therefore specified by the convolutional filter, and are learned alongside a bias. When the input is made up of multiple channels, the neuron becomes the summation of convolutional operations across all channels within the same region.

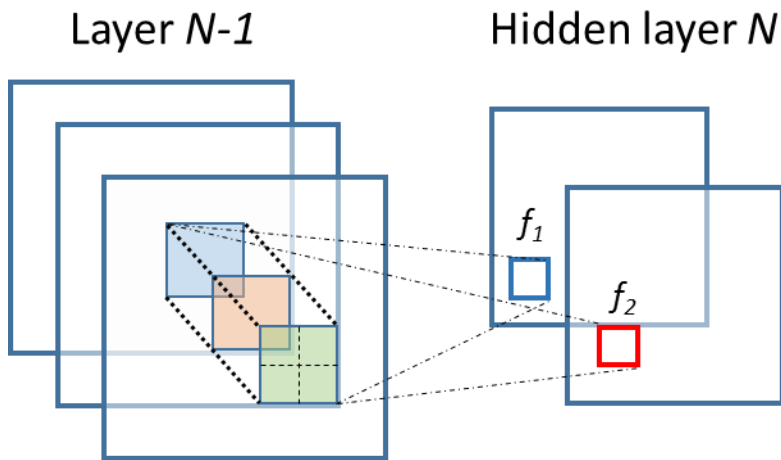


Figure 2: Diagram illustrating the relationship between the input and layers. Each resulting feature map in the hidden layer uses its own convolutional filter. The filters process the input with a sliding window that sums the convolutional results across every channel at the same coordinate.

The output of the convolutional layer feeds into a sub-sampling layer that computes a function of sub-regions of the input. The function is generally an average or maximum, and allows the layer to help create lower level percepts that consolidate the features

through a sample-based discretization process [20]. This helps prevent overfitting from highly detailed representations of the topic and reduces the complexity of the problem. The output also becomes invariant to small changes in rotation and translation [21]. Its smaller size also decreases the complexity of the problem. This layer is generally followed by a fully connected layer when performing classification problems. Convolutional neural networks are not limited to two-dimensions. Networks for multi-dimensional data are possible as long as the filter sizes are adjusted accordingly. It should be noted that a fully connected layer can be thought of as a special case of a convolutional layer, where the filter size is equal to the input size, and only a single convolution is performed.

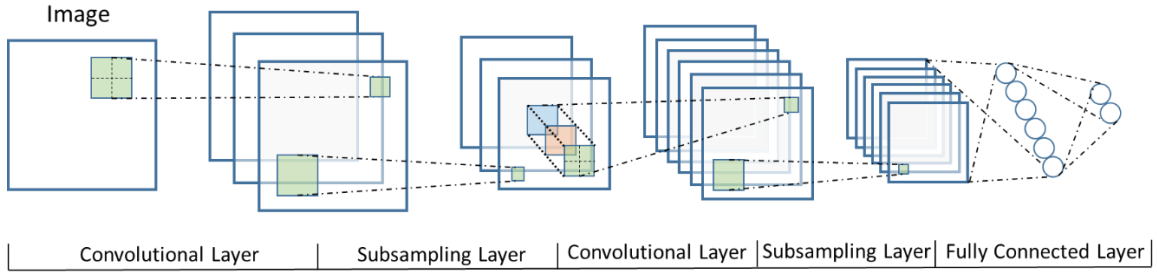


Figure 3: A visualization of the LeNet architecture. It combined convolutional, pooling, and fully connected layers to learn a model that can solve classification problems.

### 2.3. Recurrent Neural Networks

Neural networks generally work under the assumption that the inputs are independent from one another. This limits their effectiveness when applied to tasks that may require the use of sequential information. A variety of Recurrent Neural Networks (RNN) have been proposed, [21], [24], and [25], all of which create an internal network state of recurrent connections that let an imprint of previous inputs persist and affect the

evaluation of activation of current neurons, thereby allowing past data to influence current outputs (Figure 4). This means that recurrent neural networks can learn temporal patterns in data sequences. They have been applied to problems such as text generation where the network learns to predict the next character or word based on the input text sequence [38]. Unfortunately, RNNs are limited in the range of context they retain and suffer from the vanishing gradient problem, making it difficult to perform tasks with more than ten time steps between the target and relevant inputs.

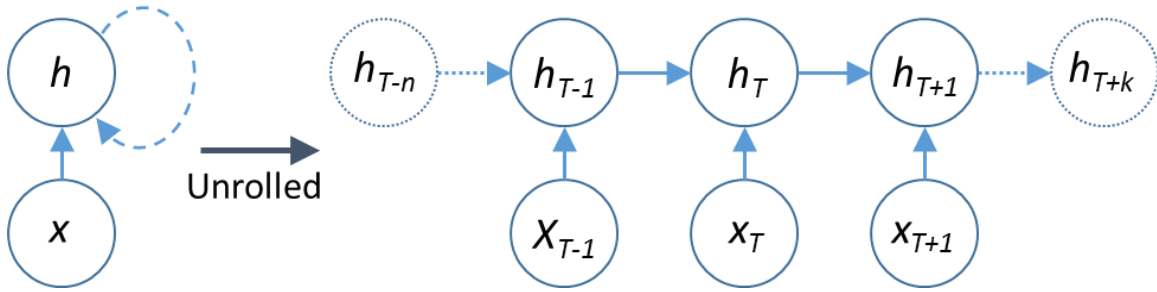


Figure 4: Unrolled Recurrent Unit

### 2.3.1 Long Short-Term Memory

The long short-term memory (LSTM) architecture seeks to overcome the limitations of the typical RNN by adding the ability to selectively remember and forget previous data. First proposed by [15], it has since been used in applications dealing with sequences that require a way to discriminatively select what should be remembered. The long short-term memory cell, as seen in Figure 5, utilizes three gates that control the information received, retained, and output by the cell to find and exploit long-term dependencies in the given data. [27]

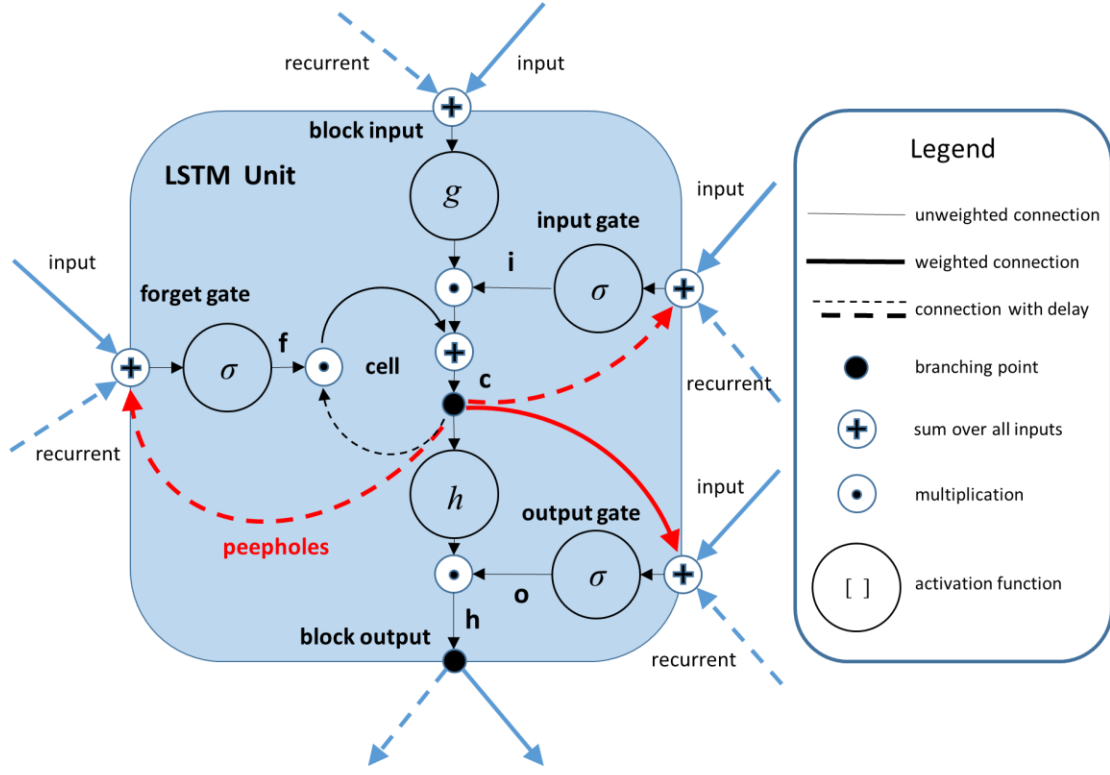


Figure 5: Long Short-term Memory Cell

There are three unique activation functions, the input, output, and gate activation functions. The former two usually use a tanh activation function, while the latter, denoted in the Figure 5 as “ $\sigma$ ”, is always a sigmoid activation function. The gate activations are calculated using a logistic sigmoid function of the dot product of the input and weights, with each gate containing its own weights. The weights are shared by the unit through each time step. The cell and hidden states are controlled by a *input and output gates*. The input gate controls whether or not the input is considered, the forget gate controls whether or not the previous cell data is considered, and the output gate controls if the current cell information is released to the next state. The formulation of the LSTM cell can be summarized as shown in (1) through (5). The inputs, outputs, and weights all represent a vector, as only element-wise multiplication, addition, and dot operations are used. Element-

wise multiplication operations are denoted by “ $\circ$ ”. The input, forget, cell, output, and hidden states for each timestep are denoted by  $i, f, c, o$ , and  $h$ , respectively,  $\sigma$  represents the activation functions, and the connections between the input and each state in the LSTM unit are denoted by a set of weights,  $W$ . The output state controls the information that is propagated from the previous timestep, while the hidden state is the actual output of the LSTM unit. The peephole connections allow the LSTM unit to access and propagate information recorded from the preceding timestep. An LSTM encoder-decoder model was used by [19] to reconstruct and predict video sequences. While It performed reasonably well on Bouncing MNIST video sequences, it was less effective on patches of natural images taken from the UCF-101 dataset [28]. The reconstructed images were fuzzy while the predictions were little more than colored blobs. This is likely due to the fact that spatial information within the data is lost while it propagates temporally though the unit. However, [28] does use the weights from the encoder trained on the UCF-101 dataset to initialize an LSTM classifier that performed well on in.

$$i_t = \sigma(W_{xi}x_t + W_{hi}h_{t-1} + W_{ci} \circ c_{t-1} + b_i) \quad (1)$$

$$f_t = \sigma(W_{xf}x_t + W_{hf}h_{t-1} + W_{cf} \circ c_{t-1} + b_f) \quad (2)$$

$$c_t = f_t \cdot c_{t-1} + i_t \circ (W_{xc}x_t + W_{hc}h_{t-1} + b_c) \quad (3)$$

$$o_t = \sigma(W_{xo}x_t + W_{ho}h_{t-1} + W_{co} \circ c_{t-1} + b_o) \quad (4)$$

$$h_t = o_t \circ \tanh(c_t) \quad (5)$$

### 2.3.2 Convolutional Long Short-term Memory

The Convolutional Long Short-term Memory architecture has been recently utilized by Shi et al. in [17] and Patraucean et al. in [18]. The Conv-LSTM units integrate convolution into

the usual fully connected LSTM (FC-LSTM) by using convolution for both input-to-hidden and hidden-to-hidden connections. The formulation of the Conv-LSTM unit can be summarized with (6) through (10). While the equations are similar in nature to (1) through (5), the input  $x$  is fed in as images, while the set of weights for every connection is replaced by convolutional filters. This allows the Conv-LSTM unit to keep track of less weights and perform convolutional operations that yield better spatial feature maps. The Conv-LSTM is more advantageous when working with images than the FC-LSTM due to its ability to propagate spatial characteristics temporally through each Conv-LSTM state.

$$I = \sigma(W_{XI} * X_t + W_{HI} * H_{t-1} + W_{CI} \circ C_{t-1} + b_I) \quad (6)$$

$$F_t = \sigma(W_{XF} * X_t + W_{HF} * H_{t-1} + W_{CF} \circ C_{t-1} + b_F) \quad (7)$$

$$C_t = F \cdot C + i_t \circ (W_{XC} * x_t + W_{HC} * h_{t-1} + b_C) \quad (8)$$

$$O_t = \sigma(W_{XO} * X_t + W_{HO} * H_{t-1} + W_{CO} \circ C_{t-1} + b_o) \quad (9)$$

$$H_t = O \circ \tanh(C_t) \quad (10)$$

Convolutional and element-wise multiplication operations are denoted by “ $*$ ” and “ $\circ$ ” respectively. Similar to the LSTM unit, the input, forget, cell, output, and hidden state of each timestep are denoted by  $I$ ,  $F$ ,  $C$ ,  $O$ , and  $H$  respectively, the activation by  $\sigma$ , and the weighted connections between states by a set of weights,  $W$ . However, each state is now a matrix representing the image, while the set of weights  $W$  is a convolutional filter. Just as the convolutional filters of the input-to-hidden connections determine the resolution of feature maps created from the input, the convolutional filter size of the hidden-to-hidden connections determine the aggregate information the Conv-LSTM unit receives from the previous time-step. The transition of states between time-steps for a Conv-LSTM unit can then be interpreted as movement between frames. Larger transitional kernels therefore

capture faster motions while smaller transitional kernels capture slower motions [17]. A visualization of the process can be seen below in Figure 6. The size of the convolutional filters in the input-to-hidden and hidden-to-hidden connections may differ depending on both the size and speed of the observed objects. The models used in [17] and [18] are able to successfully reconstruct a recognizable prediction of an input video sequence from the bouncing MNIST dataset [19]. Patraucean et al. however, does not make use of peephole connections, showing that the effectiveness of such connections in an LSTM architecture is debatable [18]. It should be noted that a FC-LSTM can be thought of as a special case of a Conv-LSTM, where the filter size is equal to the input image and only a single convolutional operation is performed, and that each Conv-LSTM unit shares the same parameter through all time-steps.

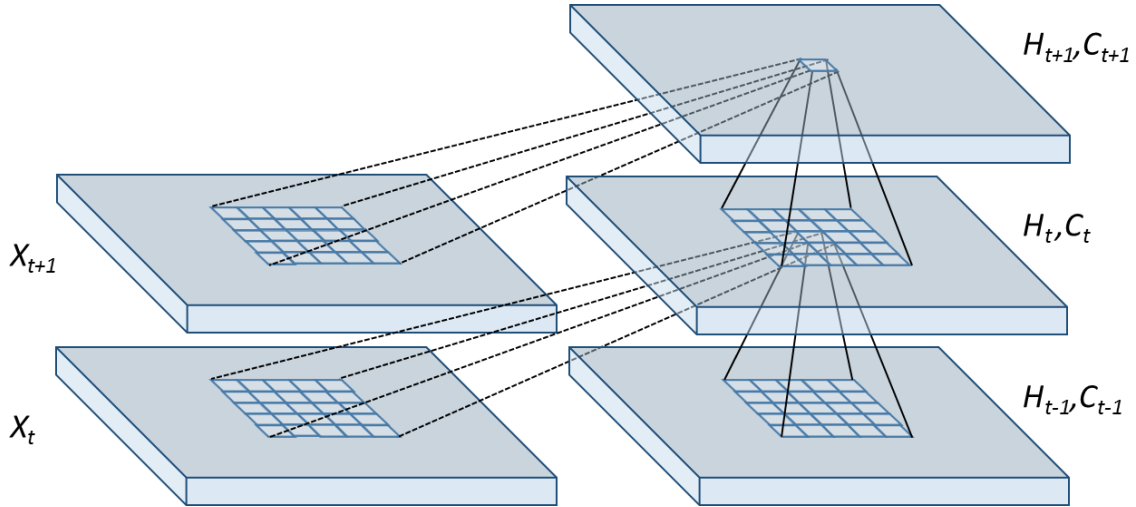


Figure 6: Inner Structure of a Conv-LSTM Unit

The models in [17] and [18] are able to successfully reconstruct a recognizable prediction of an input video sequence from the bouncing MNIST dataset [19]. The model in [18], however, does not make use of peephole connections, showing that the

effectiveness of such connections in an LSTM architecture is still unresolved. It should be noted that a FC-LSTM can be thought of as a special case of a Conv-LSTM, where the filter size is equal to the input image and only a single convolutional operation is performed.

## 2.4. Future Video Prediction

Long Short-Term Memory networks are capable of learning long-term dependencies. As such, they are able to extrapolate temporally sequential data given certain inputs. Srivastava et al. [19] takes advantage of this property to train a composite encoder-decoder model able to reconstruct the past and predict the future video sequences. More specifically, the encoder maps an input video representation to a fixed length representation, while the decoder extrapolates the learned encoding into the past and future video sequences. When using only a normal encoder-decoder model, the target values of the model determine what the model can be used for. When the target output is of the input, the model is able to create a reconstruction of the input video sequence. When the target output is of subsequent frames, however, the model learns to predict the subsequent video sequence.

The model is further improved by combining both the reconstruction and prediction models into a composite model, using both the current and future video sequences as target outputs and potentially conditioning each time-step with the output of the previous time-step (Figure 7). Reconstruction models have the tendency to learn trivial representations that merely memorize the input. Future predictors tend to absorb more information from

the most recent frames, as they are generally the most immediately relevant, i.e.,  $\{v_{t-1}, \dots, v_{t-k}\}$  are more important than  $v_0$  when predicting  $v_t$ . While this is effective for specific predictions, the loss of information from older time-steps will lead to less accurate predictions for more general video sequences during testing. The reconstruction of both the past and future video sequences forces the learned encoding to contain more meaningful data, thus improving the overall performance of the system.

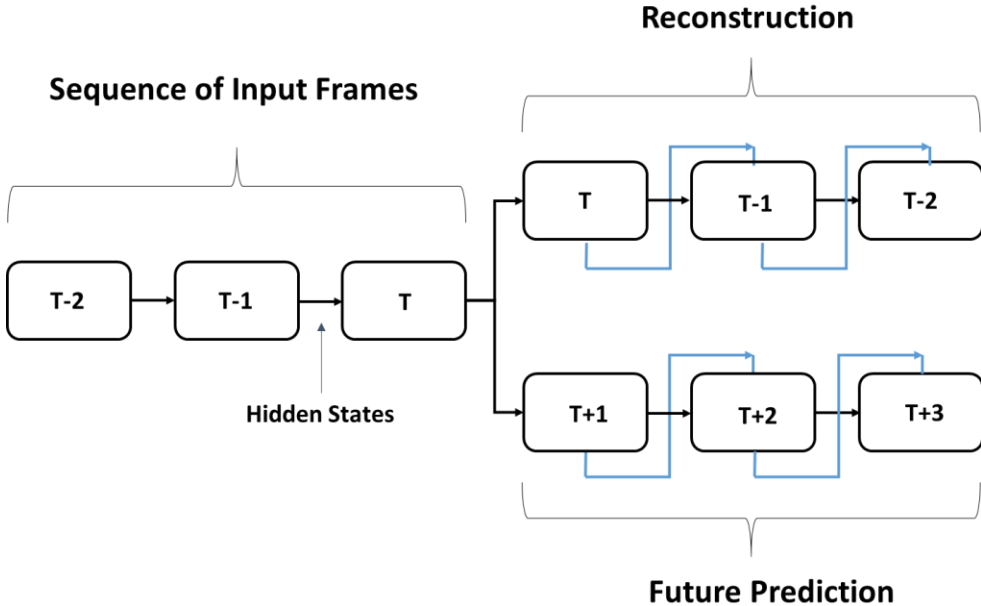


Figure 7: The composite structure for unrolled LSTM unit. Blue lines represent potential conditioning

Srivastava et al. evaluates his proposed model on the Bouncing MNIST dataset, comprised of 64x64 grayscale images (Figure 8), and a set of 32x32 natural image patches (Figure 9) from the UCF-101 dataset [28]. It is able to successfully reconstruct and predict a sequence of images accurately on the Bouncing MNIST images, with the best performance being shown by a two-layer composite model with a conditional future predictor. The model did not perform well on the natural images, with neither the

reconstruction nor the prediction maintaining spatial resolution. The input reconstruction does show a blurred approximation of both structure and motion though time, but the future prediction loses cohesion in both by the fourth time-step. While the reconstructions get sharper when more LSTM units are added to each layer, the predictions remain the same, showing the model’s inability to extrapolate the future from the encoding. The results by Srivastava et al. show that while the model is effective on simple synthetic images, it is unable to learn and temporally propagate spatial features on more complex images, regardless of size.

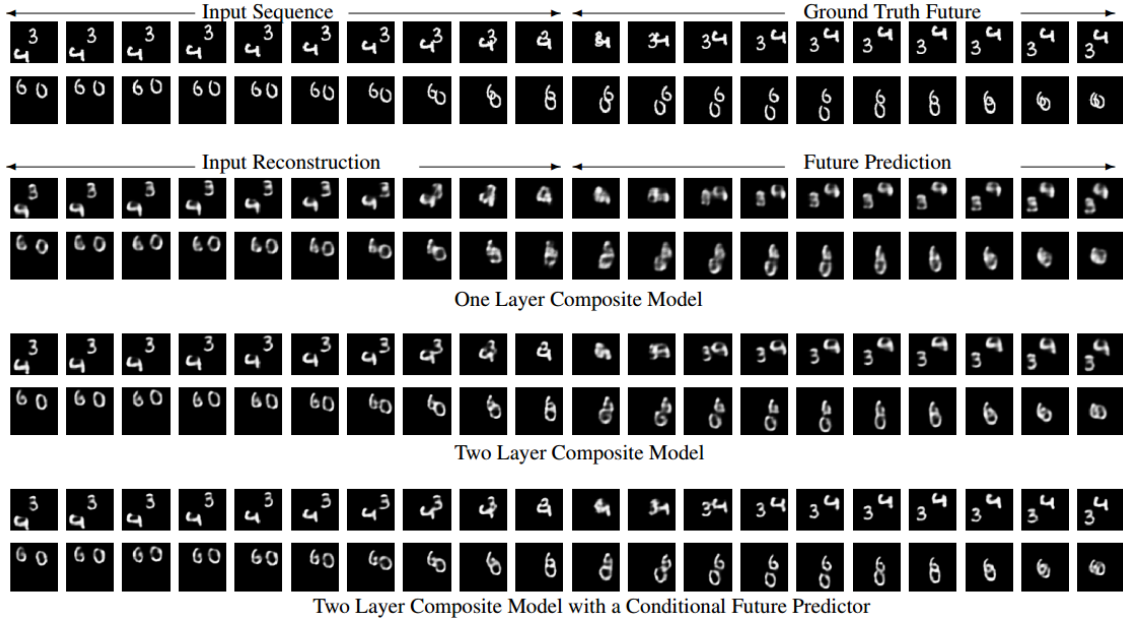


Figure 8: Re却struction and future prediction obtained from the Composite Model on a dataset of Bouncing MNIST images [19]

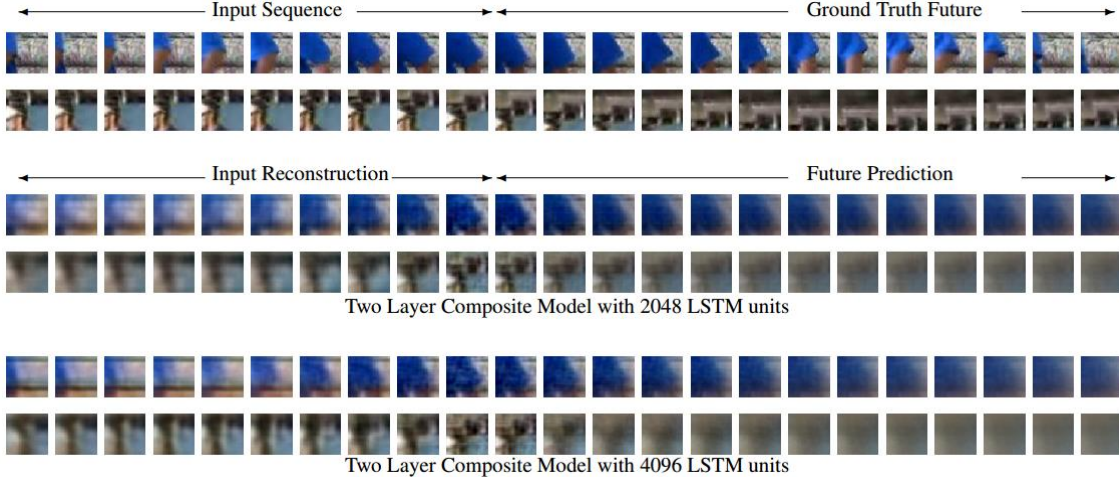


Figure 9: Reconstruction and future prediction obtained from the Composite Model on a dataset of natural image patches. [19]

Shi et al. propose the use of Convolutional LSTMs with the encoder-decoder structure for future video prediction that is able to better retain spatio-temporal information. Its decoder is unique in that it performs a  $1 \times 1$  convolutional operation across the output of each layer to obtain an output, as opposed to looking solely at the last layer. The proposed architecture was shown to outperform the LSTM models used by [19] when predicting future video sequences for a synthetic Bouncing MNIST Dataset. It was also successfully applied to a precipitation forecasting problem that used satellite imagery of clouds to predict weather patterns (Fig. 10), showing its applicability in predicting non-synthetic data.

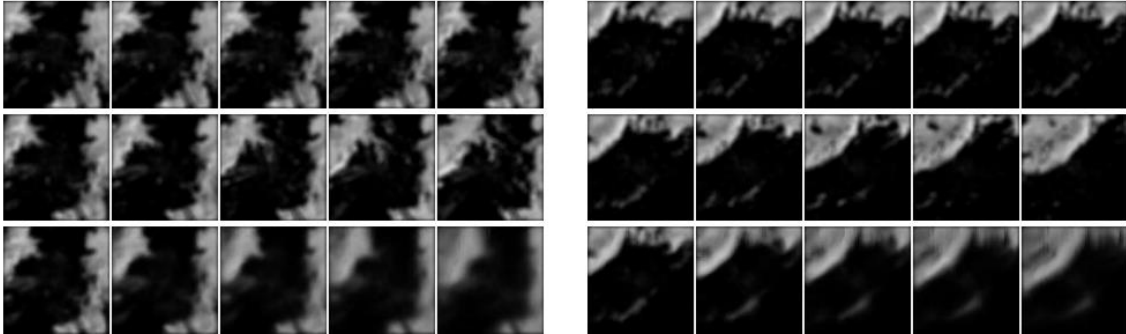


Figure 10: Two prediction examples. All of the predictions and ground truths are sampled with an interval of 3. From top to bottom: input frames; ground truth frames; prediction by the ConvLSTM forecasting network. [17]

## 2.5. *Anomaly Detection in Videos*

When labels are provided as a ground truth for anomalous actions, anomaly detection is a problem that can be evaluated by building predictive models and considering a binary classification problem. However, such labels are often uncommon, or unwieldy, and the data available for training a model are limited to containing little to no anomalous events. The available training data often result in the formulation of semi-supervised models that can be adapted to operate in an unsupervised mode by using a sample of the unlabeled data set as training data. Scoring techniques can be used to evaluate the output of the models on testing data and used to label the data using domain-specific thresholds [16].

Such techniques have been used to great effect in [5], [19], [1], [18], and [4], where models are trained with little to no supervision and used to classify anomalous sequences in a given video. Handcrafted features comprised of a mixture of dynamic textures and spatial anomaly maps are used by Cong et al. in [5] to learn the “normalcy” of a video sequence, with which an anomaly score is computed. Adam et al. does something similar

in [19] by creating a probability distribution of low-level observations. Given a new observation, it can calculate the likelihood of occurrence to determine whether or not it is anomalous. The issue with hand-crafted features is that they may be too specialized, which makes them unable to adapt to or learn unexpected events effectively. Neural networks deal with this issue by allowing the network to learn what features are important. Zhao et al. utilizes an unsupervised dynamic sparse coding algorithm in [1] to train dictionaries with which anomalies are detected through the reconstruction error. Lu et al. improves upon this in [18] by introducing an approach that directly learns sparse combinations instead of a dictionary, thereby significantly speeding up testing. While sparse coding has been shown to be effective, dictionaries may still contain unused or noisy elements within the dictionary, reducing their effectiveness. Hasan et al. employs a convolutional neural network in [4] to learn the temporal regularity of given video sequences. A regularity score is computed from the reconstruction error and used to detect anomalous segments. While effective, convolutional neural networks were not developed with temporal features in mind, and are related to Conv-LSTMs as dense networks are related to LSTMs.

## **Chapter 3 Anomaly Detection through Future Prediction**

This chapter describes the approach used to perform anomaly detection through future prediction using convolutional long short-term memory units. The proposed approach is inspired by the idea that an encoder-decoder model will be able to learn and reconstruct “regular” video sequences from the training data. This will force anomalous data to be more difficult to reconstruct with each subsequent time-step due to error propagation. The design of the proposed architectures used to predict future video sequences are discussed in Section 3.1, and the evaluation algorithms used to identify anomalous video segments is discussed in Section 3.2.

### **3.1. *Proposed Architectures***

Convolutional LSTM (Conv-LSTM) units have recently been proposed and used by [17] and [18] (Section 2.3.2). It takes advantage of the spatial information retained by training convolutional weights to better propagate spatial features temporally in the LSTM. These units have been utilized to create two distinct network architectures, a Composite Conv-LSTM Encoder Decoder, described in Section 3.1.1, and a Composite Conv-LSTM Autoencoder, described in Section 3.1.2. The results can be found in Section 4.

#### **3.1.1 Proposed Composite Convolutional LSTM Encoder-Decoder**

The architecture is inspired by the models discussed in Section 2.4. The network by Shi et al. utilizes only a future encoding-decoder model to predict future video sequences, while the model by Srivastava et al. utilizes a composite conditioned structure, but is comprised of FC-LSTM units. The proposed architecture utilizes multiple stacked Conv-LSTM layers in an end-to-end trainable network. The design is split into two main

parts, the encoder, and the decoder. A high level view of the proposed model using three Conv-LSTM layers can be seen in Figure 11.

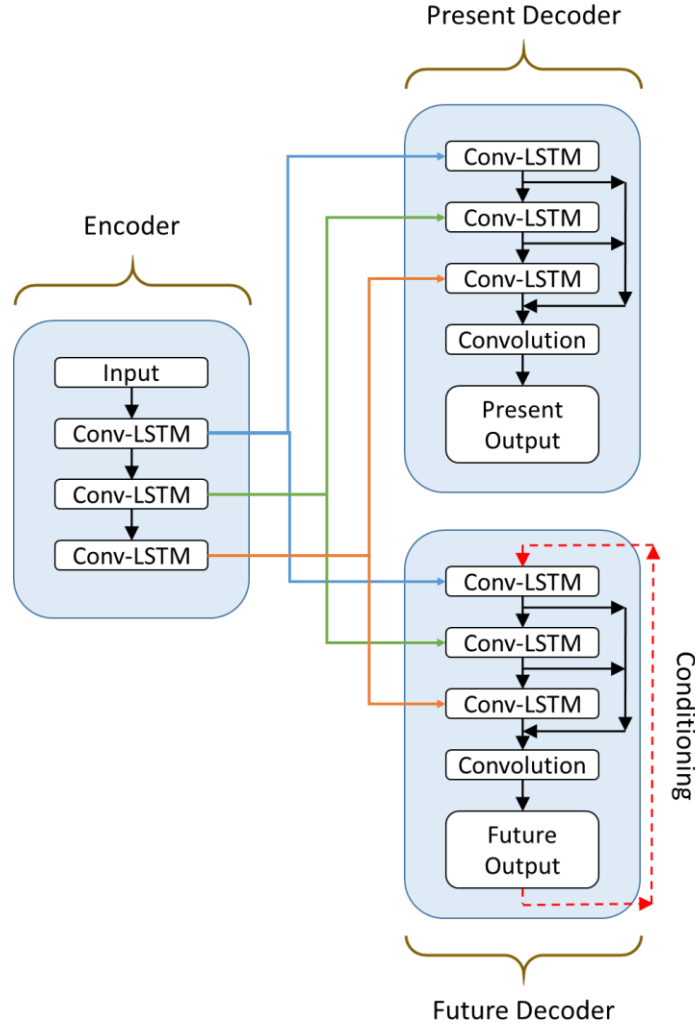


Figure 11: High-level view of the Conditioned Composite Conv-LSTM Encoder-Decoder. The right side is the encoder, while the left is the decoder. The decoder is split into a present and future decoder, where the future decoder is potentially conditioned with the output of the current time-step feeding into the input of the next.

### 3.1.1.1 Encoder

The encoder accepts a sequence of reshaped frames in chronological order as input. Images contain redundant information. By reshaping the input into a stack of non-

overlapping patches, the model will lose detail but learn more significant data. Each Conv-LSTM layer is made up of multiple Conv-LSTM units that span across the specified number of time-steps. The outputs of the last time-step of each Conv-LSTM layer are used as the encoding. Unlike traditional convolutional neural networks [10], the proposed model does not utilize max-pooling layers. It instead feeds the output of each Conv-LSTM layer directly into the next one, allowing each subsequent layer to accrue temporal changes and focus on different features.

### 3.1.1.2 Decoder

The decoder is split into two parts, the past, and the future. The past decoder reconstructs the input video segment, while the future decoder creates a prediction of what the future video segment will be. The first time-step of both portions of the decoder are initialized with the same encoding provided by the corresponding layers of the encoder. The past decoder does not use anything as input to the first layer, and the output is determined solely from the information extracted from its initialization. The outputs of each layer are concatenated together and summed through a 1x1 convolutional filter to obtain the reconstruction of the input. This final step essentially forces each layer to represent the same set of input patches at different temporal features. The first layer is the most static and will focus on still objects while the last layer will focus on larger movements. We consider two options for the future decoder, one in which it is not conditioned, and one in which it is. An unconditioned decoder has the same architecture as the past decoder. A conditioned decoder uses the summed output of each time-step as the input to the first layer of the subsequent time-step, thus “conditioning” it to the previous frame.

As stated in [19], only the future decoder is conditioned, because the past only has one possible outcome, while the future may vary. Conditioning potentially limits the variation by providing more information from the previous time-step. The proposed architecture uses a composite conditioned structure comprised of Conv-LSTM units. By combining the approaches taken by Shi et al. and Srivastava et al., a better prediction can be obtained for more accurate reconstruction errors. This potentially allows the model to better learn a video’s normality, thus making anomalous video segments containing sequences that are hard to reconstruct more likely to stand out.

### 3.1.2 Proposed Conv-LSTM Autoencoder

This architecture is inspired by the convolutional autoencoder network used by Hasan et al, and is adapted for future prediction by the inclusion of an additional encoder. The proposed architecture utilizes multiple stacked Conv-LSTM layers in conjunction with max-pooling layers in an end-to-end trainable model. The design utilizes a two-step encoder-decoder format, where the decoder is structured as an autoencoder (Fig. 12). The finalized design utilizes a composite structure.

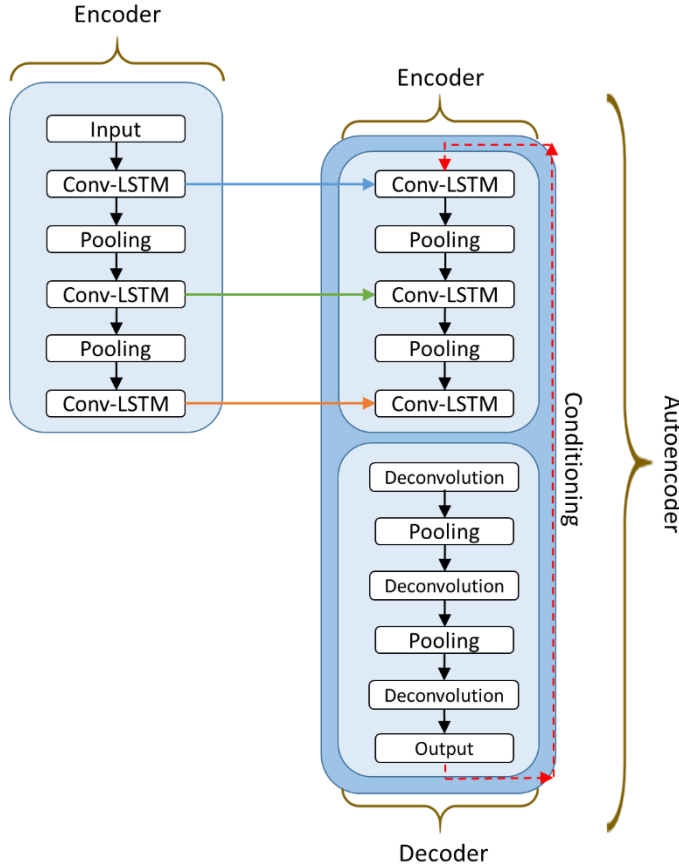


Figure 12: High-level view of the Conditioned Conv-LSTM Autoencoder. The right side is the encoder, while the left is the decoder. The decoder uses an autoencoder format and is conditioned with the output of the current time-step feeding into the input of the next. The full composite model has a duplicate of the decoder with the target output being the input frames.

### 3.1.2.1 Encoder

A sequence of frames is used as input to the first Conv-LSTM layer. It is then immediately followed by a max-pooling layer. The max-pooling layer helps consolidate the activation of neurons representing the features while increasing spatial invariance and reducing dimensionality. The output is then fed back into any additional Conv-LSTM layers, with the process repeating. This allows the features within large images to be found and meaningfully compressed. The hidden outputs of the last time-step of each Conv-

LSTM layer is an encoding and used to initialize the corresponding Conv-LSTM layers of the decoder.

### 3.1.2.2 Decoder

The decoder employs an autoencoder structure, with its own encoder and decoder. The encoder portion utilizes the same structure as the first encoder, but initializes its Conv-LSTM layers with the encoding of the corresponding layer from the encoder. This encoder is responsible for transforming the initialization into a traditional convolutional autoencoder encoding at each time-step. The new encoding at each time-step is decoded through deconvolution followed by unpooling layers to restore the image to its former size. The deconvolution weights are tied to the input-to-cell convolutional weights from the respective Conv-LSTM layer. Two decoders are also employed, one for the past input video sequence, and one for the future prediction. As with the Encoder Decoder model, we consider both an unconditional and a conditional structure for the future decoder. The conditioned decoder accepts the output of the last layer in the previous time-step as the input to the first layer of the current time-step.

It should be noted that this architecture does not utilize tied weights between the encoding and decoding portions of the autoencoder. This is due to the fact that the input of the encoder portion is not the same as the output of the decoder, as the architecture extrapolates the future.

### 3.1.3 Parameters of Note

The proposed architecture has many more parameters than a convolutional or LSTM network. For the structure of the architecture, these parameters include the filter

size of each connection in a Conv-LSTM unit, the number of Conv-LSTM units in a layer, the number of layers, the input and target segment lengths, and the patch size by which a frame is reshaped.

The number of Conv-LSTM layers is important in that it determines the number of chances temporal information have to be transmitted in a model. For instance, the third time-step in the first layer could only receive information from the input and the previous two time-steps. The same time-step at the third layer would receive the same, but the input of each time-step from the second layer may receive information from the previous time-steps of that layer. At the same time, only so many layers can be added before the data propagated through time becomes redundant. The input-to-hidden filters serve a similar purpose to the convolutional filters in traditional convolutional neural networks. As discussed in Section 2.3.2 however, the filter size of hidden-to-hidden connections is responsible for both controlling the propagation of information between states and capturing motion between frames. It is therefore important to examine the speed of objects in the target domain when selecting this parameter.

The input and target lengths determine the amount of information to be encoded and extrapolated, respectively. The longer the input length is, the more information it will have to learn, i.e. what data is meaningful and should be propagated into the encoding. At the same time, this comes at the cost of additional parameters that increase the memory and computational cost. Conversely, a longer output requires more information to be extrapolated from a single encoding. The patch size determines the complexity of the model. A large patch size will result in more detailed feature maps. However, not all spatio-temporal features are unique. Movement by larger or similar objects can often be broken

down into smaller motions that can be modeled together. A larger patch size is therefore more likely to produce more noise and contain non-essential information.

It is also important to select a proper non-linearity function to prevent the issue of vanishing gradients, a suitable loss function to calculate the deviation between the target and model outputs, and an appropriate update function to learn weights efficiently.

### **3.2. Evaluation Algorithm**

A trained model can be used to obtain a reconstruction of the input video sequence and prediction of its subsequent frames. This reconstruction can be visualized for a qualitative inspection by the user, or quantified for use in evaluation algorithms. In a qualitative inspection of the reconstruction and predictions, anomalous events will be more likely to stand out, as the trained model does not have the necessary information to properly reconstruct or predict it. For a quantitative assessment, the reconstruction and prediction errors will be recorded and used in an evaluation algorithm. The reconstruction error,  $e$ , is obtained by taking the total Mean Squared Error (MSE) as defined in Eq. (11), where  $\hat{\theta}$  is the pixel value of the model's output,  $\theta$  is the target value,  $n$  is the number of pixels per frame, and  $p$  is the number of frames.

$$e = \sum_{k=1}^n \sum_{i=1}^p (\hat{\theta}_{ki} - \theta_{ki})^2 \quad (11)$$

The quantitative evaluation algorithm used in this thesis is based on the one used by [19]. A regularity score is computed from the error values. The regularity score normalizes the error of the reconstruction between zero and one with respect to the other

reconstructions from the same video, as different videos may have different notions of abnormality. The regularity  $g(x)$  of a sequence can be computed as follows:

$$g(x) = 1 - \frac{e(x) - \min_x e(x)}{\max_x e(x)} \quad (12)$$

where  $x$  is the output reconstruction sequence and  $e(x)$  is the reconstruction error of that sequence. Video sequences containing normal events will have a high regularity score since it is similar to the data used to train the model, while sequences containing abnormal events will have a low regularity score. Abnormal events will cause the prediction reconstructions to diverge further from the target output, as the model will not contain information to support it. Distinct local minima or scores below a certain threshold from a time series of regularity scores can therefore be used to determine the location of abnormal video sequences.

This thesis improves upon the methodology by Hasan et al. by using Conv-LSTMs to learn better spatio-temporal features and making use of both distinct local minima and maxima within the evaluation algorithm to determine anomalous regions more accurately. The distinct points are found with a filter using the Persistence 1D algorithm [30]. The algorithm finds such points by finding local minima and maxima after smoothing the function using a biharmonic reconstruction. Distinct local minima represent video sequences that are highly likely to contain anomalies. Regions of anomalous video segments are proposed based on the minima found. Points that are within a certain threshold can be considered to be part of the same anomalous sequence. Distinct local maxima potentially represent regular video sequences that take place immediately before or after an anomalous one. These points help decrease the number of false positives by

limiting the length of the proposed anomalous segment. More specifically, the new proposed region border is midway between the maxima and minima. This constraint is precluded when the distinct maxima is between two distinct minima that are considered to be of the same anomalous sequence. The proposed anomalous regions are recorded for every video evaluated and compared to the ground truth. Anomalies are considered detected if a certain percentage of the proposed detection is overlapped by the ground truth anomaly. Multiple detections of the same anomaly are considered a single true positive detection.

### 3.2.1 Parameters of Note

The evaluation algorithm has several tunable parameters. The length of the proposed anomalous segment directly impacts how likely it is for it to overlap the ground truth anomalous segment. A large area may include the actual anomaly, but contain large sequences of data that are normal. Conversely, it is more likely for a small area to include only the anomalous region, but is less likely to do so and may not encompass the entire thing. The overlap percentage is responsible for determining if the proposed anomalies are actually anomalies. A low percentage means that it would be correct even if only a tiny portion of the proposal is correct, while a high percentage would require very high precision for it to match the ground truth. The distance by which two distinct minima would be considered of the same anomaly ties into this by affecting the area of the anomalous segment, as it merges the proposed segments based on both minima.

The most important parameter is the threshold used in the Persistence 1D algorithm to filter distinct minima and maxima. Each distinct minimum represents a potential

anomalous video segment, while each distinct maximum helps constrain the regions for more accuracy. It should be noted that the evaluation algorithm is more likely to be accurate in longer video clips. Shorter videos are more likely to have anomalies near the beginning or end of the video, thus reducing the amount of information provided and making it harder for the anomaly to be recognized.

## **Chapter 4    Experimental Results**

### **4.1. *Experimental Setup***

The proposed system is designed, coded, and trained using Lasagne. Lasagne is a lightweight library used to build and train neural networks in Theano. Its supports many different neural network implementations including, but not limited to, dense networks, Convolutional Neural Networks, and recurrent networks. It is also highly modular with every part able to be used independently of Lasagne, transparent with its source code easily understandable and available in Python, and easily modified. The last part is especially important, as the source code for the Conv-LSTM unit used in [6] was not yet available when work for this thesis was started. Caffe was considered but not chosen. While it is easy to implement existing networks in Caffe, it is much more difficult to modify the source code. Classes in Lasagne were modified to allow for a Conditioned Encoder-Decoder implementation of a Conv-LSTM network.

MATLAB was chosen as the tool used to evaluate the model outputs and detect anomalies. It is a powerful tool that allows for a quick visualization of both the regularity scores and reconstructions. A prototype of each proposed network was first tested and evaluated to ensure that the code written was working as intended. The proposed networks were then evaluated to determine the most effective one. The best model was then trained and evaluated over multiple datasets. The outputs were analyzed qualitatively through a visualization of the past reconstruction and future prediction, and quantitatively by comparing the average loss and detection rates. Matlab was used to visualize the evaluations.

#### 4.1.1 Dataset Selection

The datasets used in the experiments are the Bouncing MNIST dataset [19], UCSD Pedestrian Datasets [8], Avenue Dataset [14], and Subway Datasets [3]. The results used for comparison were obtained from [15] and [9].

The Bouncing MNIST dataset is a synthetic dataset comprised of 10,000 video sequences, with each sequence depicting two MNIST [21] figures moving around in a 64x64 pixel area, and 20 frames long (Figure 13). It is used by [17] and [19] to show that their models are able to predict and reconstruct future video sequences.

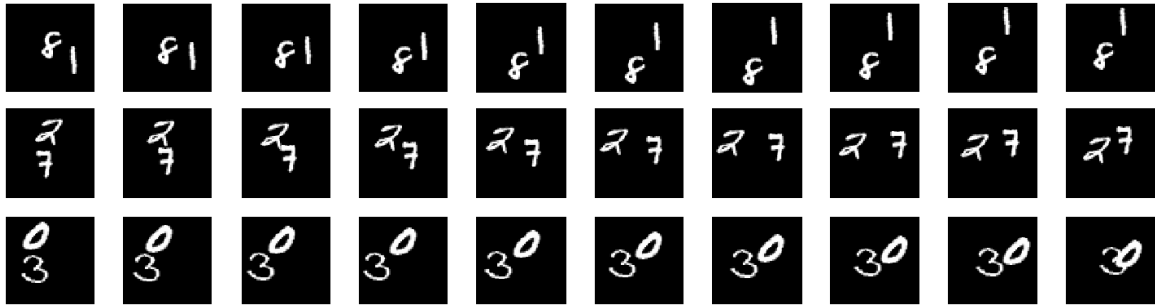


Figure 13: Three samples of the first ten frames from three sequences of the Bouncing MNIST dataset

The UCSD Pedestrian dataset is comprised of two subsets, Pedestrian 1 and Pedestrian 2, that each depict the activities of a different pedestrian walkway and are further split into training and testing data. The training data contains only the “regular” activity of pedestrians, while the test data contains “anomalous” events including but not limited to people skateboarding, cycling, and driving small vehicles (Figure 14).

The Subway dataset is split into two subsets, Enter and Exit (Figure 15). The first subset depicts people entering a subway station, while the second shows them leaving. They are both also split further into training and testing data.



Figure 14: Images from the UCSD Pedestrian dataset. The left and right columns are from the Pedestrian 1 and 2 subsets respectively.



Figure 15: Images from the Subway dataset. The left and right columns are from the Exit and Entrance videos respectively.

The Avenue dataset captures activity on a CUHK campus avenue (Figure 16). The images are in RGB and contain images of activity that are generally larger than those found in the UCSD and Subway datasets. Like the other two, it also contains both a training and testing dataset.



Figure 16: Images from the Avenue Dataset.

The Bouncing MNIST dataset is only evaluated on the baseline Future Conv-LSTM Encoder Decoder model seen in Section 2.4. As it was also used by [17] and [19] in their experiments, the preliminary results obtained from it are used as a benchmark to ensure that the base code is working correctly. While useful as an initial validation for the base network code, it is unable to show whether or not the model is applicable to the problem explored in this thesis. The Bouncing MNIST dataset is synthetic and simplistic, while the videos relevant to the problem domain are all natural footage.

The UCSD Pedestrian 1 dataset was chosen as the benchmark dataset for all experiments done in this thesis. It is used to find the most effective model by tuning the parameters discussed in Section 4.3.1. Once the optimal model was found, it was then evaluated on the UCSD Pedestrian 2, Avenue, and Subway datasets.

## 4.2. Preliminary Code Validation

Prototypes of the encoder-decoder and autoencoder networks that are only able to perform future prediction are evaluated on Bouncing MNIST data. The initial parameters selected for the preliminary future Conv-LSTM encoder-decoder used to evaluate the Bouncing MNIST (BMNIST) dataset are based on the parameters used in [17]. The convolutional filter size used for both the input-to-hidden and hidden-to-hidden connections was 5x5. Since the target pixels are either black or white, a sigmoid nonlinearity was applied to the output of the convolutional layer, and a binary cross entropy was used as the loss function. Three Conv-LSTM layers were used, with 256, 128, and 128 filters respectively. As in [6], RMSProp [31] with a learning rate of  $10^{-4}$  and decay rate of 0.9 is used. An input and output length of five frames each was selected, as the accuracy of the reconstructions is prioritized over an abstraction of predicted motion. As the parameters for the Conv-LSTM Autoencoder model are similar, the same parameters are chosen for use when applicable.

The models are compared with an implementation of the precipitation forecasting model used by Shi et al. While it is not stated in [17], the released code by Shi et al. also reconstructs the output of the last time-step of the input. A comparison of the average binary cross entropy per frame between the model output and ground truth, as seen in Table 1, would show that the forecasting model performed the best while the autoencoder model performed the worst. This is misleading because it averages in the input reconstruction output of the encoder. A visualization of the outputs in Figure 17 shows that output of the encoder-decoder model has a much higher resolution than the autoencoder model, whose output becomes increasingly blurred with every subsequent time-step. As the networks

were evaluated to make sure the code was written correctly, they were only trained using a mini-batch for 20,000 iterations, and the parameters were not optimized.

Table 1: A comparison of Loss between the prototype networks trained on the Bouncing MNIST dataset

	Average Binary Cross Entropy Per Frame
Encoder-Decoder Model	238.406
Precipitation Forecasting Model	219.587
Autoencoder Model	261.256

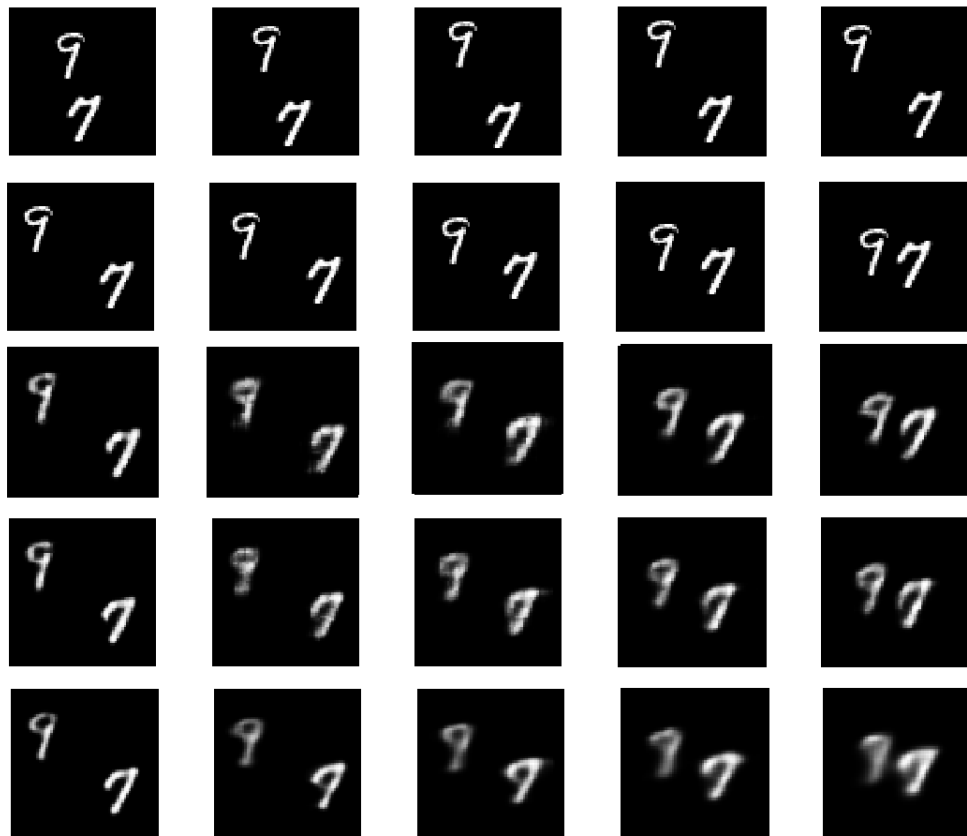


Figure 17: A comparison between prototype network outputs. Each column denotes a time-step sequentially from left to right starting at T+1. Each row from top to bottom represent the input sequence, the target ground truth future sequence, the forecasting model [17], the encoder-decoder prototype, and the autoencoder prototype.

## **4.3. Parameter Selection**

### **4.3.1 Model Parameters**

The input images are resized to 224x224 pixels and converted to grayscale. A preliminary Conv-LSTM Encoder-Decoder baseline model was evaluated for use as reference in parameter selection. The baseline model utilizes parameters similar to the prototypes tested in Section 4.2, with an input length of five, output length of five, a filter size of 5x5, three Conv-LSTM layers, and a total of 512 Conv-LSTM filters. A sigmoid non-linearity is also applied to the final convolutional layer.

The parameters tested in variations of the baseline model include the length of both the input and output, the filter size, and the non-linearity function (Table 2). The model with an input length of ten outputs a slightly lower MSE per frame, but takes 1.5 times the amount of time to train, making it largely inefficient. Furthermore, the more time-steps into the future the model predicts, the worse each prediction becomes (Table 1). A filter size of 3x3 was considered as the objects in the datasets utilized move more slowly than the one used by [17]. As most convolutional neural networks use a rectified linear unit (ReLU) nonlinearity function, that is tested as well. Ultimately, the parameters used by the baseline model are shown to be the most effective. As the parameters for the Conv-LSTM Autoencoder model are similar, the same parameters are chosen for use when applicable.

The binary cross entropy loss function is not suitable for natural images like those seen in the UCSD Pedestrian dataset. The loss function for the baseline model is therefore changed to Mean Square Error. All other parameters remain the same. Evaluations using other parameters are done with respect to the baseline model.

The parameters changed include the number of layers, and the number of Conv-LSTM units per layer. While traditional convolutional layers apply a rectified linear unit (ReLU) nonlinearity to the output, a sigmoid nonlinearity is also considered. The total number of units remain the same though, (i.e., one layer has 512 units, while two layers may have 256 units in each). The input and output length are set at ten for two different experiments. The best model parameters are then used to evaluate a composite and conditioned composite model.

Table 2: Comparing reconstruction accuracy performance

Parameters Modified (Input Length, Output Length, Filter Size, Output Nonlinearity)	Average MSE Per Frame
(5, 5, 5x5, Sigmoid)	20.5076
(10, 5, 5x5, Sigmoid)	17.46702
(5, 10, 5x5, Sigmoid)	23.0266
(10, 10, 5x5, Sigmoid)	24.8644
(5, 5, 3x3, Sigmoid)	30.183
(5, 5, 5x5, ReLU)	24.8302

For the UCSD Pedestrian 1 and 2 datasets, the last training video sample was held out for validation. For the Subway and Avenue datasets that have only one video for training, the last twentieth of the video was held out for use as validation. Early stopping based on validation loss was applied to all experiments.

### 4.3.1.1 Optimization and Initialization

The cost function of eq. (11) was optimized with RMSProp [31]. It uses a running average over the root mean squared of recent gradients to normalize the gradients and divide the learning rate. A learning rate of  $10^{-3}$  and decay rate of 0.9 are used. Adagrad [33] and Adam [34] were both considered and tested as well, but RMSProp was empirically chosen for its smaller resulting loss values. The learning rate is set to .0001. We use a mini-batch of five video sequences and train the models for up to 25,000 iterations. Early stopping is performed based on the validation loss if necessary. The weights are initialized using the Xavier algorithm [35]. The algorithm automatically scales the initialization based on the number of input and output neurons to prevent the weights from starting out too small or large. This is significant, as weights that start too small cause a reduction of variance in the output that propagate a decrease in both the weights and values until they become too small to matter. Similarly, too large of a starting weight will cause the learned weights and outputs to explode in magnitude [31]. It is also an important factor in speeding up and ensuring the convergence of the network. The convolutional filters within the input-to-hidden and hidden-to-hidden states in the Conv-LSTM units all use the same filter size in this thesis. It should be noted that while units share the same parameters at each timestep, the filter sizes of different states within the unit may differ in size if necessary.

### 4.3.2 Evaluation Parameters

A temporal window of fifty frames before and after distinct local minima is used to propose anomalous regions, as most anomalous activities are approximately one hundred frames long. The proposed regions of local minima within fifty frames of one another are joined to obtain the final abnormal temporal regions. These minima are then considered to

be a part of same abnormal event. We consider a detected abnormal region as a correct detection if it has at least fifty percent overlap with the ground truth. A parameter-sweep at intervals of 0.05 is performed to determine the threshold parameter for the Persistence1D algorithm [30]. Since abnormal events are unique to each target video domain, a different threshold is selected for each dataset.

To make the results easier to visualize, the regularity score and its evaluation are graphed. Distinct local minima are represented by a blue dot, distinct local maxima are represented by a red dot, the anomalous ground truth regions are highlighted in red, and the proposed anomalous regions are highlighted in green. It should be noted that the last nine frames are not evaluated since the model requires a minimum of ten frames, five as the input and five as the target, to return a reconstruction score.

## 4.4. Results

### 4.4.1 Predicting Past and Future Video Sequences

The learned models are able to successfully reconstruct the past and predict the future. The encoder-decoder based model performs significantly better than the autoencoder based models (Table 3), with the former an average MSE per frame of less than a tenth of the latter. Contrary to our expectations, the unconditioned model performed slightly better than the conditioned version. We were not able to test the conditioned composite autoencoder model due to time constraints.

We visualize the output to qualitatively analyze the capabilities of both network models. For ease of visualization, the composite output of each network is split into two

figures, one for the input reconstruction, and one for the future prediction. The autoencoder model produces a much blurrier output showing that it is only able to learn a vague impression of both shape and motion through time from the data it has been trained on. In Figures 18 and 19, it can be seen that the both the input reconstruction and the future prediction of the autoencoder model are unable to learn the finer details needed to differentiate pedestrians from one another. The resolution of each pedestrian at every time-step seem to be equal.

Table 3: Comparing reconstruction accuracy performance

Model	Avg. MSE per Frame
Composite Encoder-Decoder	14.8321
Conditioned Composite	16.0691
Autoencoder Composite Model	28.1933

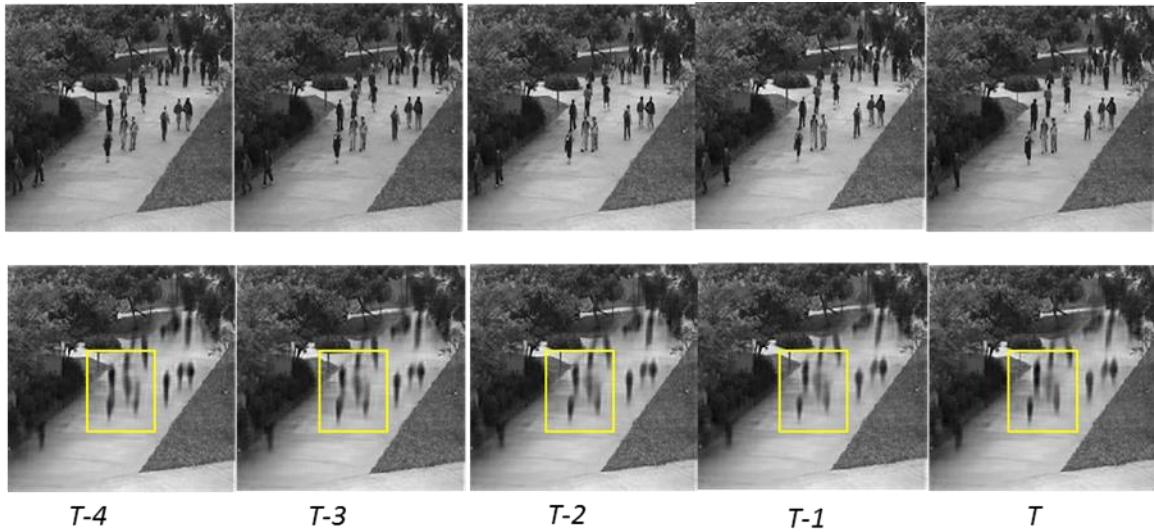


Figure 18: Input reconstruction obtained from the Composite Conv-LSTM Autoencoder Model on a *non-anomalous* sequence from test clip 1 of the UCSD Pedestrian 1 dataset. The first row is the input ground truth video sequences, while the second is the input reconstruction. Each column denotes a time-step. Regions of interest that change through time are highlighted by a yellow bounding box.

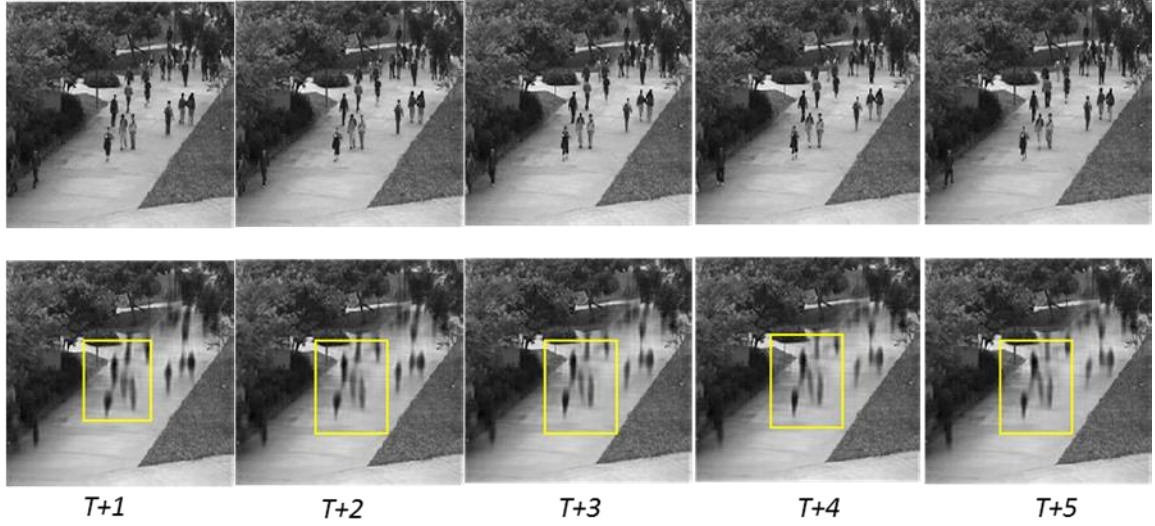


Figure 19: Future prediction obtained from the Composite Conv-LSTM Autoencoder Model on the *non-anomalous* sequence from test clip 1 of the UCSD Pedestrian 1 dataset used in Figure 18. The first row is the future ground truth video sequences, while the second is the output prediction. Each column denotes a time-step. Regions of interest that change through time are highlighted by a yellow bounding box.

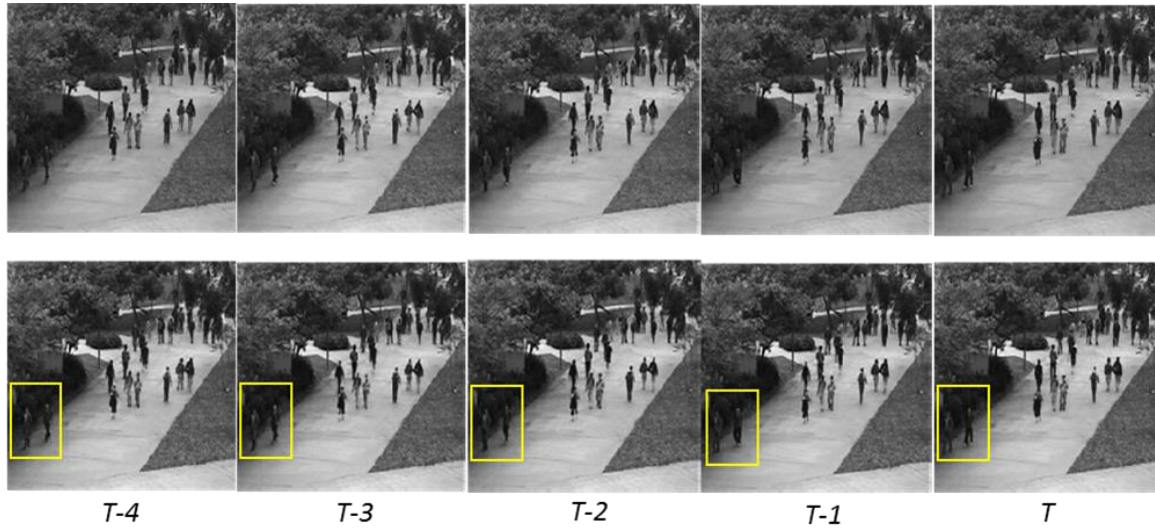


Figure 20: Input reconstruction obtained from the Composite Conv-LSTM Encoder-Decoder Model on a *non-anomalous* sequence from test clip 1 of the UCSD Pedestrian 1 dataset. The first row is the input ground truth video sequences, while the second is the input reconstruction. Each column denotes a time-step. Regions of interest that change through time are highlighted by a yellow bounding box.

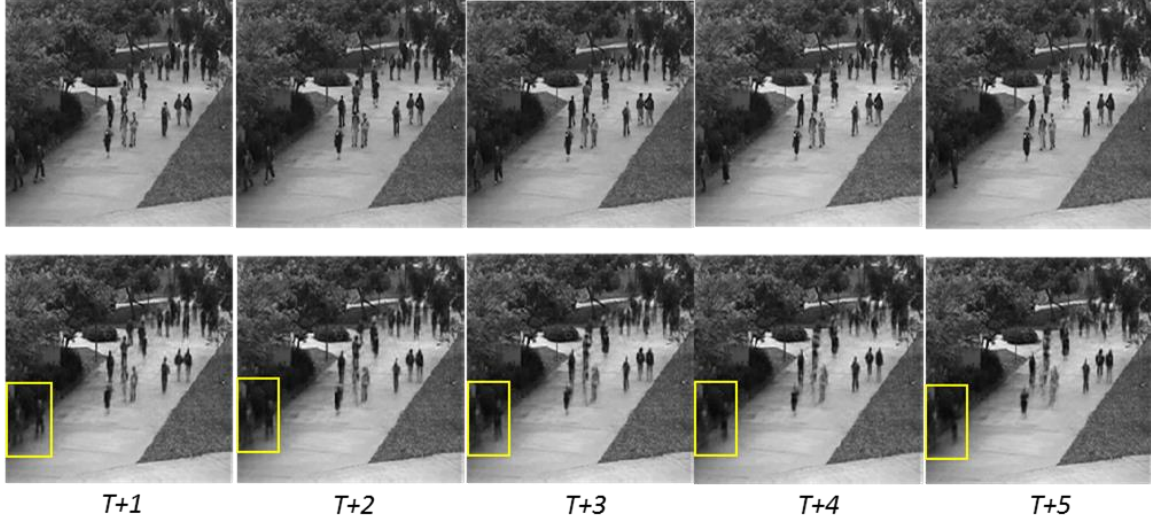


Figure 21: Future prediction obtained from the Composite Conv-LSTM Encoder-Decoder Model on the *non-anomalous* sequence from test clip 1 of the UCSD Pedestrian 1 dataset used in Figure 20. The first row is the future ground truth video sequences, while the second is the output prediction. Each column denotes a time-step. Regions of interest that change through time are highlighted by a yellow bounding box.

Figures 20 and 21 display the output of the unconditioned composite encoder-decoder model. The ground truth video sequence is of a regular event in which only pedestrians are walking across the pavement. The input reconstruction is shown to be slightly more accurate than the future prediction. The pedestrians on the walkway lose very little resolution even at the last reconstructed time-step. It can also be seen that the position of each pedestrian’s feet changes at each time-step to match the ground truth. The encoder-decoder model is able to successfully predict the input video sequence’s next five frames with the output at time-steps T+1 through T+5 containing a fairly accurate rendition of the ground truth. Although the figures of some pedestrians begin to blur slightly at T+2, the position of each pedestrian’s feet can be clearly seen to slowly move between frames even at T+5. The model is shown to reconstruct the input and predict the future of a “normal”

video sequence. We must then investigate the network’s ability to model “anomalous” events within a given video sequence.

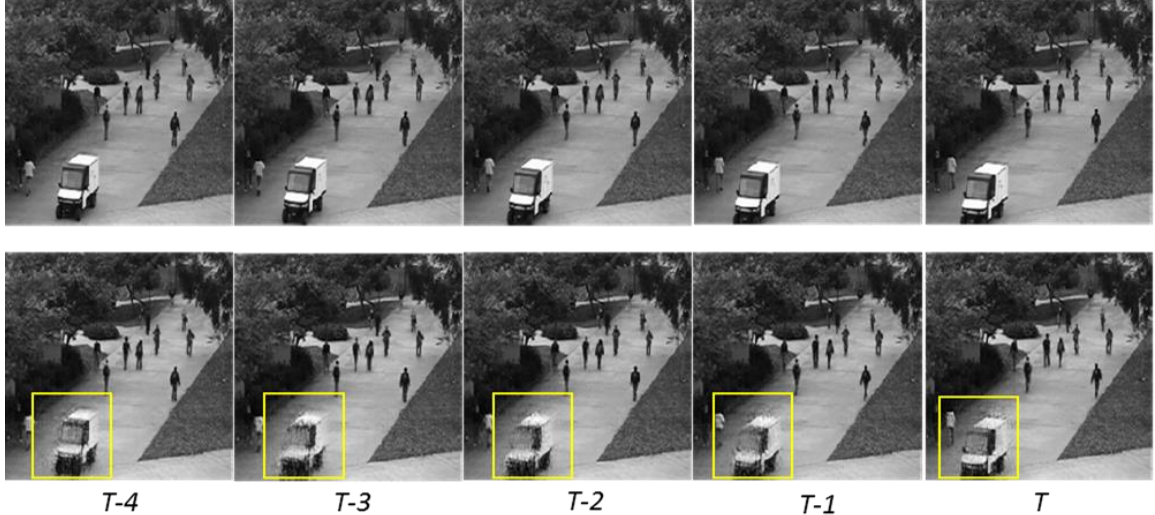


Figure 22: Input reconstruction obtained from the Composite Conv-LSTM Encoder-Decoder Model on an *anomalous* sequence from test clip 1 of the UCSD Pedestrian 1 dataset. The first row is the input ground truth video sequences, while the second is the input reconstruction. Each column denotes a time-step. Regions of interest that change through time are highlighted by a yellow bounding box.

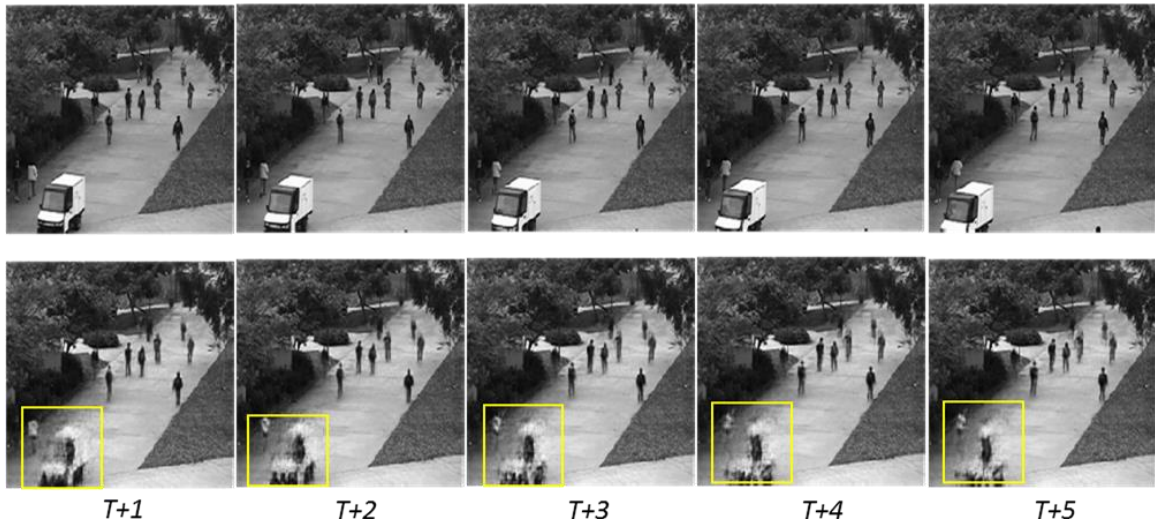


Figure 23: Future prediction obtained from the Composite Conv-LSTM Encoder-Decoder Model on the *anomalous* sequence from test clip 1 of the UCSD Pedestrian 1 dataset used in Figure 22. The first row is the future ground truth video sequences, while the second is the output prediction. Each column denotes a time-step. Regions of interest that change through time are highlighted by a yellow bounding box.

The small vehicle seen in Figures 22 and 23 does not belong on a pedestrian walkway. As such, it is “anomalous” and unable to be reconstructed or predicted properly. It can be seen that the reconstruction of pedestrians walking, a normal event, within the anomalous sequence is portrayed correctly by the model, while the small vehicle loses detail with each time-step. The past reconstruction of the vehicle is more accurate because all of the information is already within the encoding. However, the reconstruction of the small vehicle is noticeably affected by both blur and noise. The future prediction of the vehicle is already distorted at T+1. Each successive time-step significantly deteriorates its shape and motion. In fact, because the model has only learned to extrapolate the motion of pedestrians, the shape of the vehicle begins to look increasingly similar to pedestrian with every subsequent time-step.

Figures 24 and 25 contain a biker riding down the walkway. The biker’s figure in the input reconstruction is less clear than the pedestrians around him. The figure becomes even blurrier within the model prediction output. The bicycle’s shape merges with the biker’s with each time-step, and he begins to resemble a pedestrian. Moreover, the biker’s position changes more slowly than his ground truth counterpart. The visualization of output video sequences from the UCSD Pedestrian 1 dataset make it clear that the model will be able to accurately reconstruct and predict only “normal” events that were learned during training.

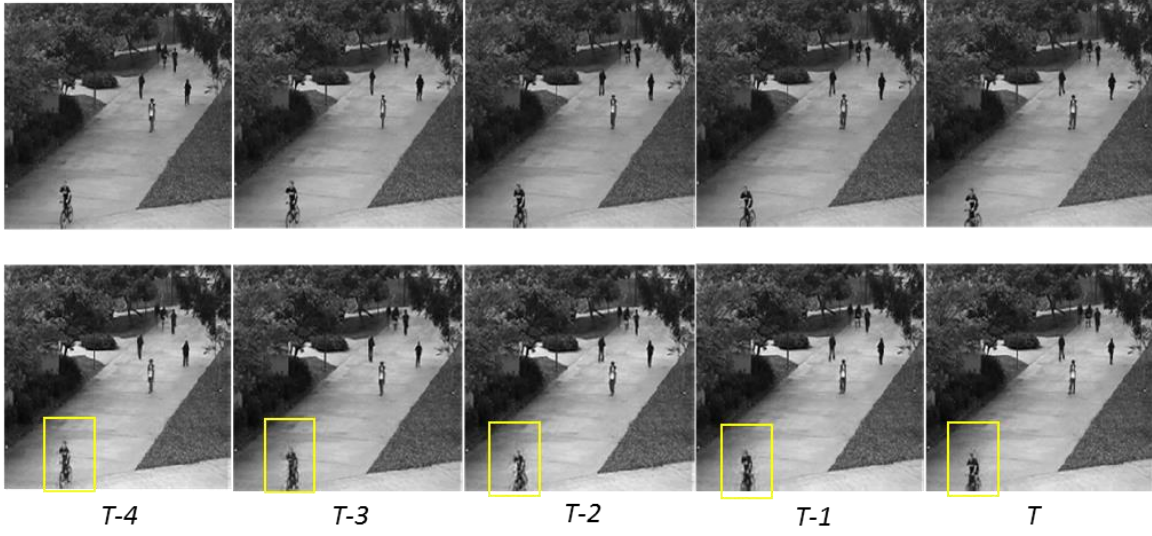


Figure 24: Input reconstruction obtained from the Composite Conv-LSTM Encoder-Decoder Model on an *anomalous* sequence from test clip 29 of the UCSD Pedestrian 1 dataset. The first row is the input ground truth video sequences, while the second is the input reconstruction. Each column denotes a time-step. Regions of interest that change through time are highlighted by a yellow bounding box.

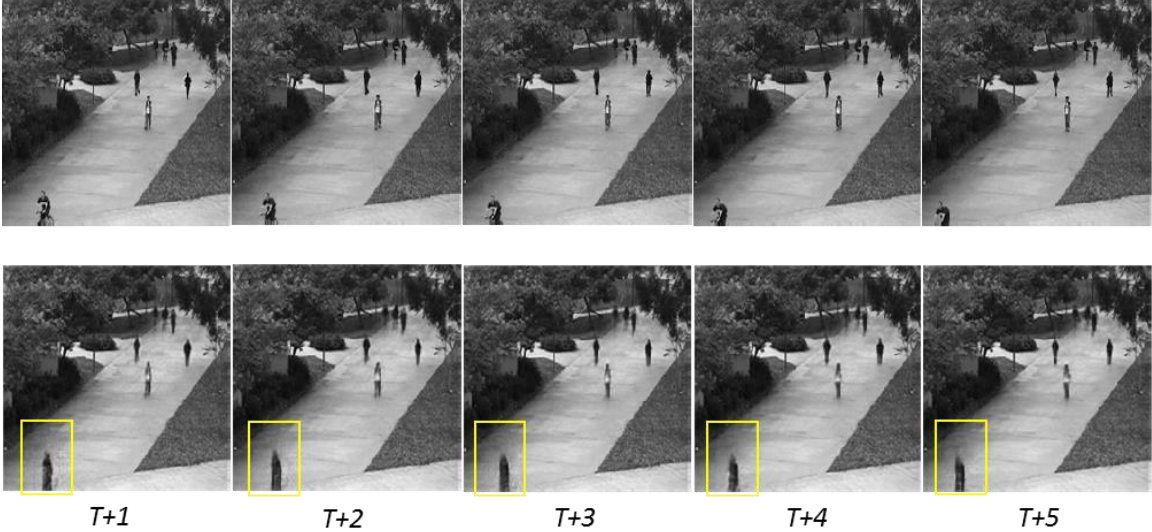


Figure 25: Future prediction obtained from the Composite Conv-LSTM Encoder-Decoder Model on the *anomalous* sequence from test clip 29 of the UCSD Pedestrian 1 dataset used in Figure 24. The first row is the future ground truth video sequences, while the second is the output prediction. Each column denotes a time-step. Regions of interest that change through time are highlighted by a yellow bounding box

#### **4.4.2 Preliminary Anomaly Detection Evaluation**

The proposed models are trained and evaluated the UCSD Pedestrian 1 dataset for an initial evaluation. The best model is chosen and improved. The best model is then further evaluated on the remaining datasets. The datasets used are discussed alongside the evaluation results.

##### **4.4.2.1 UCSD Pedestrian 1**

This dataset is split into training and testing data. It contains a variety of abnormal events that can be categorized into two main categories, the movement of non-pedestrian entities, and anomalous pedestrian motions. Common anomalies include bikers, skaters, and people walking perpendicular to the walkway, or off of it. The crowd densities range from sparse to very crowded, providing a wide range of regular actions. No anomalies occur within the training data, while at least one anomaly occurs per testing clip.

The anomaly detection results for the proposed models are shown in Table 4. Both of the proposed models are outperformed by the model in [15]. Furthermore, the conditioned and unconditioned versions of the encoder-decoder model exhibit similar detection rates. We focus on improving the unconditioned composite encoder-decoder model, as it shows the best performance.

#### **4.4.3 Improved Anomaly Detection Evaluation**

We speculate that the performance of the encoder-decoder based model can be improved by compressing the size of the input to reduce the reconstruction error. An improved model using input video frames that are downsized to 64x64 pixels is proposed. The number of overlapping patches the image is split into for the model is reduced to 16 to

compensate for the reduced image size. Since, the size of both objects and range of motions within the video decrease, we train the model using a 3x3 filter as well, and choose the parameter providing the smallest reconstruction error (Table 5). The improved Conv-LSTM Encoder-Decoder model is shown to outperform the state of the art model (Table 4). The unconditioned model has one more true positive detection than the conditioned version, increasing its recall rate to 100%.

It should be noted that while the proposed models yield between six and eight false positives, a closer examination shows that the ground truth annotation is actually incomplete, as it is missing several instances of pedestrians walking off of the walkway and has at least one corrupted video frame. We keep the same ground truth annotation so that the proposed models can be fairly compared with the one by Hasan et al.

Table 4: Comparing anomaly detection performance of the proposed models on UCSD Pedestrian 1 dataset. There are a total of 40 anomalous events.

	TP/FP	Precision	Recall
Ground Truth	40/0	1.00	1.00
Composite Autoencoder	32/8	.80	.80
Composite Encoder-Decoder (224x224)	35/8	.81	.88
Conditioned Composite Encoder-Decoder (224x224)	35/7	.83	.88
State of the Art [4]	38/6	.864	.95
Composite Encoder-Decoder (64x64)	40/7	.851	1.00
Conditioned Composite Encoder-Decoder (64x64)	39/7	.848	.975

Table 5: Average MSE per frame when evaluated on 64x64 pixel images using the specified parameters

	3x3 filter	5x5 filter
Composite Encoder-Decoder	0.569657	0.346889
Conditioned Composite Encoder-Decoder	0.687243	0.413605

Figure 26 shows a comparison between the regularity scores obtained from the original and improved network models for test clip 36 from the UCSD Pedestrian 1 dataset. The improved model visibly decreases the regularity of irregular events while increasing the regularity of segments that are correctly defined as “normal.” While the change may not seem significant, the increase in contrast between both types of events makes the distinct maxima and minima stand out more, allowing for a more accurate assessment of the video sequences.

The evaluation algorithm used to process regularity scores is used on test clip 29 from the UCSD Pedestrian 1 dataset (Figure 27). It can be clearly seen that the two anomalous events of someone biking on the walkway are denoted by large dips in the regularity score centered on the distinct minima found at frames 1 and 94, and that the distinct maximum helps to constrain the anomalous event detected to the correctly specified region. When inspecting the decrease in regularity for both clips 36 and 29, we find that the gradual decrease is caused by the way the video captures the anomalous object moving along the walkway. The irregular events begin at the top-right of the frame and end at the bottom-left for these two clips, making them larger at the end. The smaller regularity score at the end of the event indicates that larger anomalous objects tend to be more easily detected by the network. This is supported by the fact that larger anomalous

objects will produce a larger reconstruction error, as they take up a larger portion of the image. A visualization of results from the model anomaly detection evaluation on six other clips from the UCSD Pedestrian 1 dataset can be found in Figure 28.

The proposed model performs very well on the UCSD Pedestrian 1 dataset because there is sufficient data on what the accepted definition of normality is. It contains many variations of pedestrian activities ranging from a single person walking slowly to a group moving along. Furthermore, there are few abnormal events that occur in the training data.

Table 6: Comparing abnormal event detection performance across multiple datasets. Ours is the Composite Conv-LSTM Encoder-Decoder (64x64) model. \* Improved ground truth on Subway Exit dataset. # Uses older dataset.

		Dataset				
		UCSD Ped 1	UCSD Ped 2	Subway Enter	Subway Exit	Avenue
	# Frames	7,200	2,010	121,749	64,901	
	# Anomalous Events	40	12	66	19	30*
True Positive/ False Alarm	Ours	40/7	12/1	62/14	19/37	29/15
	[15]	38/6	12/1	61/15	17/5	
	[14]	N/A	N/A	57/4	19/2	
	[9]	N/A	N/A	60/5	19/2	
Precision	Ours	.851	.923	.816	.339	.659
	[15]	.864	.923	.803	.773	
	[14]	N/A	N/A	.934	.904	
	[9]	N/A	N/A	.923	.904	
Recall	Ours	1.00	1.00	.939	1.00	.964
	[15]	.95	1.00	.92	.895	
	[14]	N/A	N/A	.864	1.00`	
	[9]	N/A	N/A	.909	1.00	

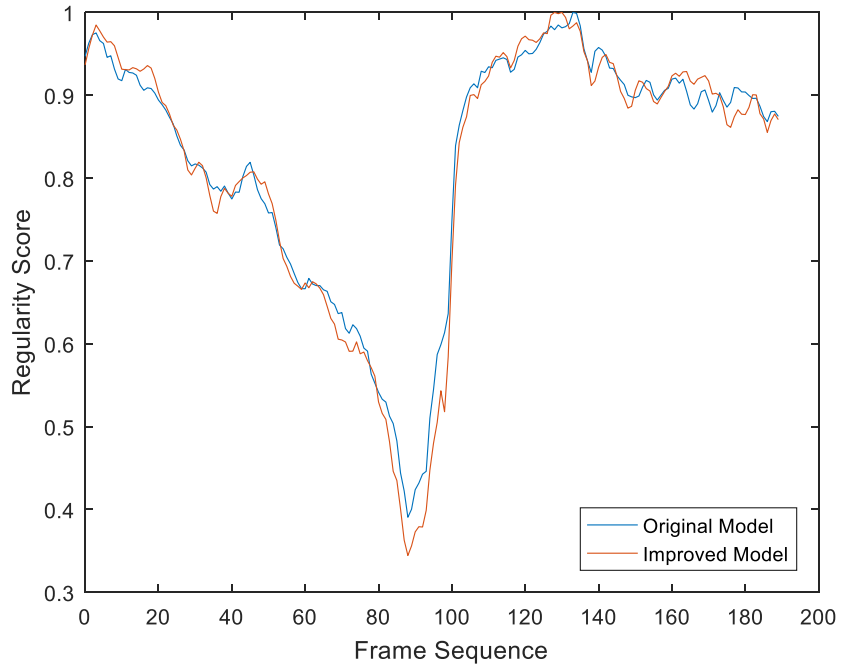


Figure 26: A comparison between the original and improved model's regularity scores for testing clip 36 of the UCSD Pedestrian 1 dataset.

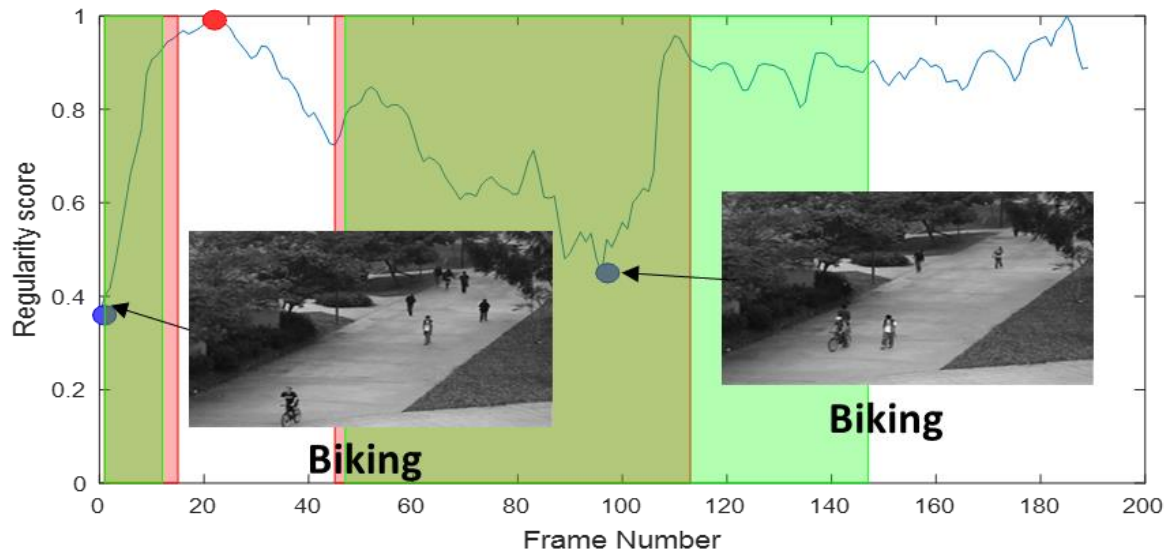


Figure 27: Regularity score (Eq.7) of test clip 29 of the UCSD Pedestrian 1 dataset. Distinct local minima are represented by a blue dot, distinct local maxima by a red dot, the anomalous ground truth regions are highlighted in red, and the proposed anomalous regions are highlighted in green.

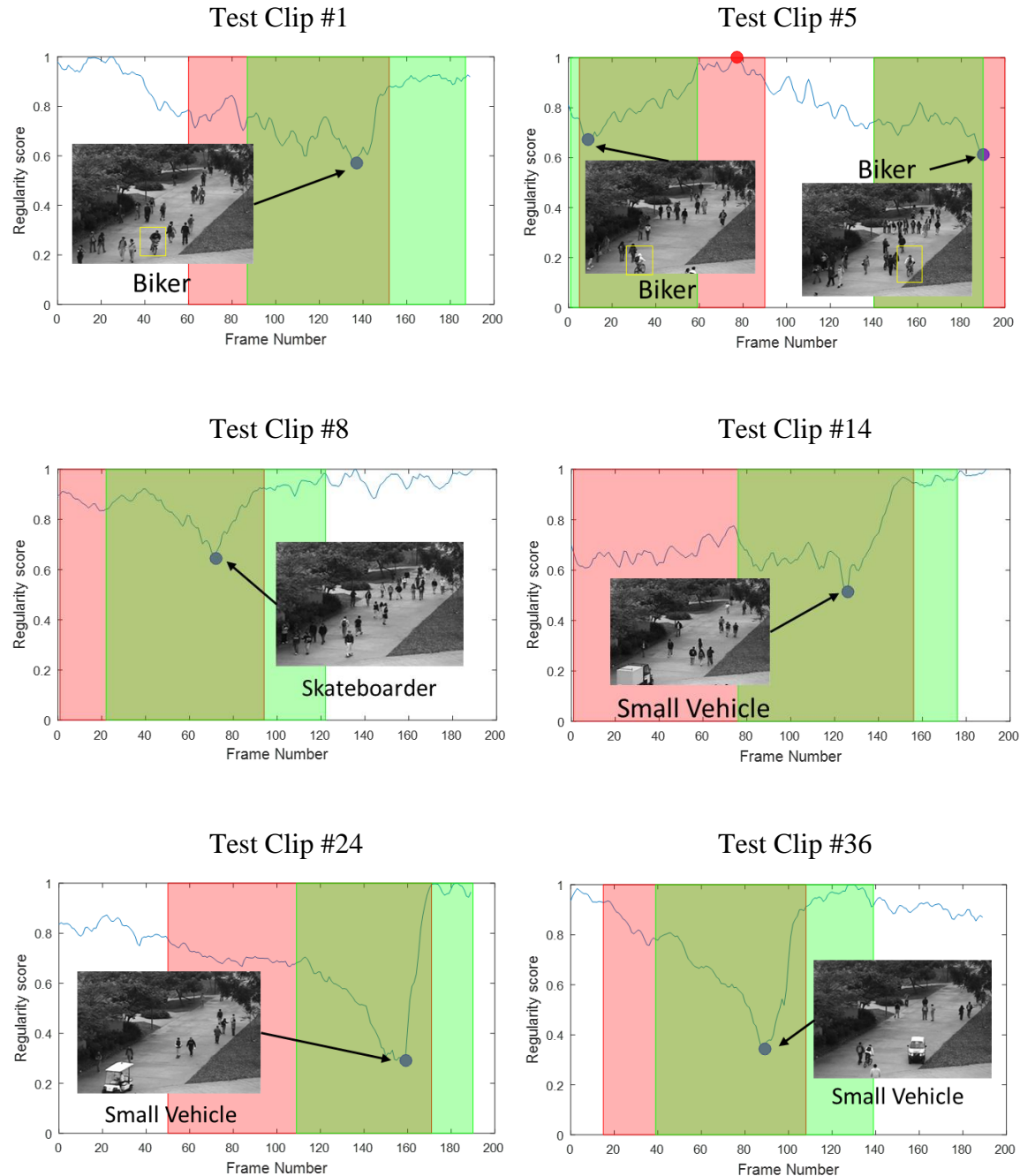


Figure 28: Anomaly evaluation graphs of test clips from the UCSD Pedestrian 1 dataset. Smaller areas of interest are highlighted with a yellow bounding box.

As the Unconditioned Composite Conv-LSTM Encoder-Decoder model exhibits the best performance, we further evaluate it on the rest of the datasets for a comprehensive quantitative evaluation (Table 6). We provide state-of-the-art results from Hasan et al. [15], Lu et al. [14], and Zhao et al. [9] for comparison. To the best of our knowledge however, only Hasan et al. reports correct detection or false alarm results by event for UCSD Ped1 and Ped2 datasets in the literature, while the state-of-the-art results for the Avenue dataset from [14] are not directly comparable as it is reported on the older and smaller version of the Avenue dataset. A comprehensive discussion of the results for each dataset can be found in Sections 4.4.3.1 – 4.4.3.4.

#### 4.4.3.1     UCSD Pedestrian 2

This dataset is similar in content to UCSD Pedestrian 1. However, it features a different walkway at a level angle, and contains fewer anomalies. There is only one abnormal event per testing clip, with most of the anomalies spanning the majority of the video segment. The proposed model is able to learn the regular motion of pedestrians walking and differentiate it from any abnormalities. There is a 100% recall rate with only one false positive on this dataset. Unlike the previously discussed dataset, the regularity score of abnormal events in the UCSD Pedestrian 2 dataset is generally even throughout (Figure 29), because the size of the anomalous object remains relatively constant throughout the sequence. A visualization of results from the model anomaly detection evaluation on six other clips from the UCSD Pedestrian 2 dataset can be found in Figure 30. We also qualitatively examine the effects of anomalies on the model reconstructions and predictions. Because a visualization of a 64x64 image is too low resolution to perform any meaningful analysis, we display the outputs of our original composite Conv-LSTM

encoder-decoder model for an anomalous event at a 224x224 resolution (Figures 31 – 32).

As seen in previous reconstructions, the pedestrians are more detailed than the irregular biker. The wheels of the bike are not complete and missing some parts. The prediction in the UCSD Pedestrian 2 dataset is blurrier than the ones seen for the UCSD Pedestrian 1 dataset. However, it is evident that Figure 32 correctly captures the shape and motion of the pedestrians while slowly eroding the shape of the bicycle with every time-step.

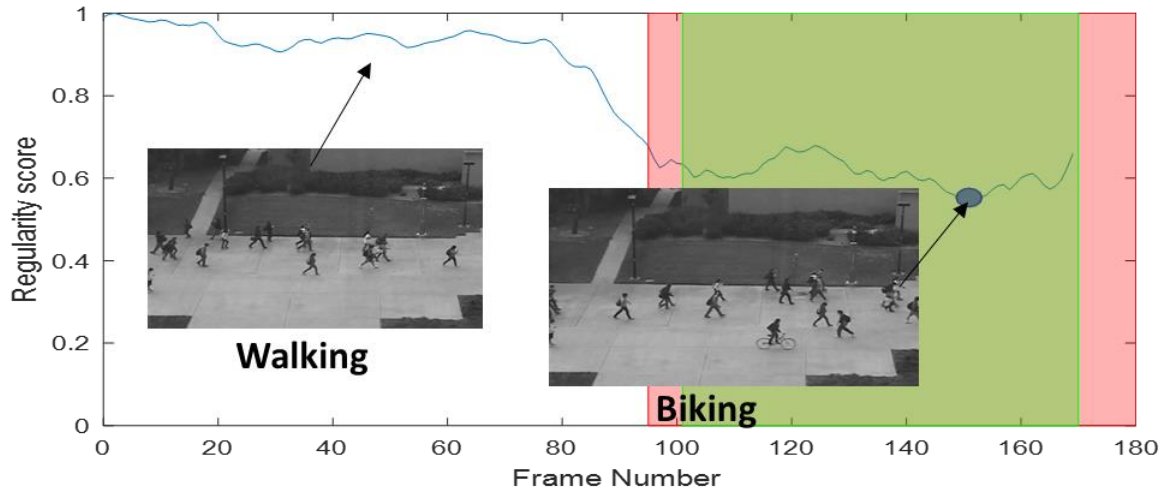


Figure 29: Regularity score (Eq.7) of test clip #2 of the UCSD Pedestrian 2 dataset

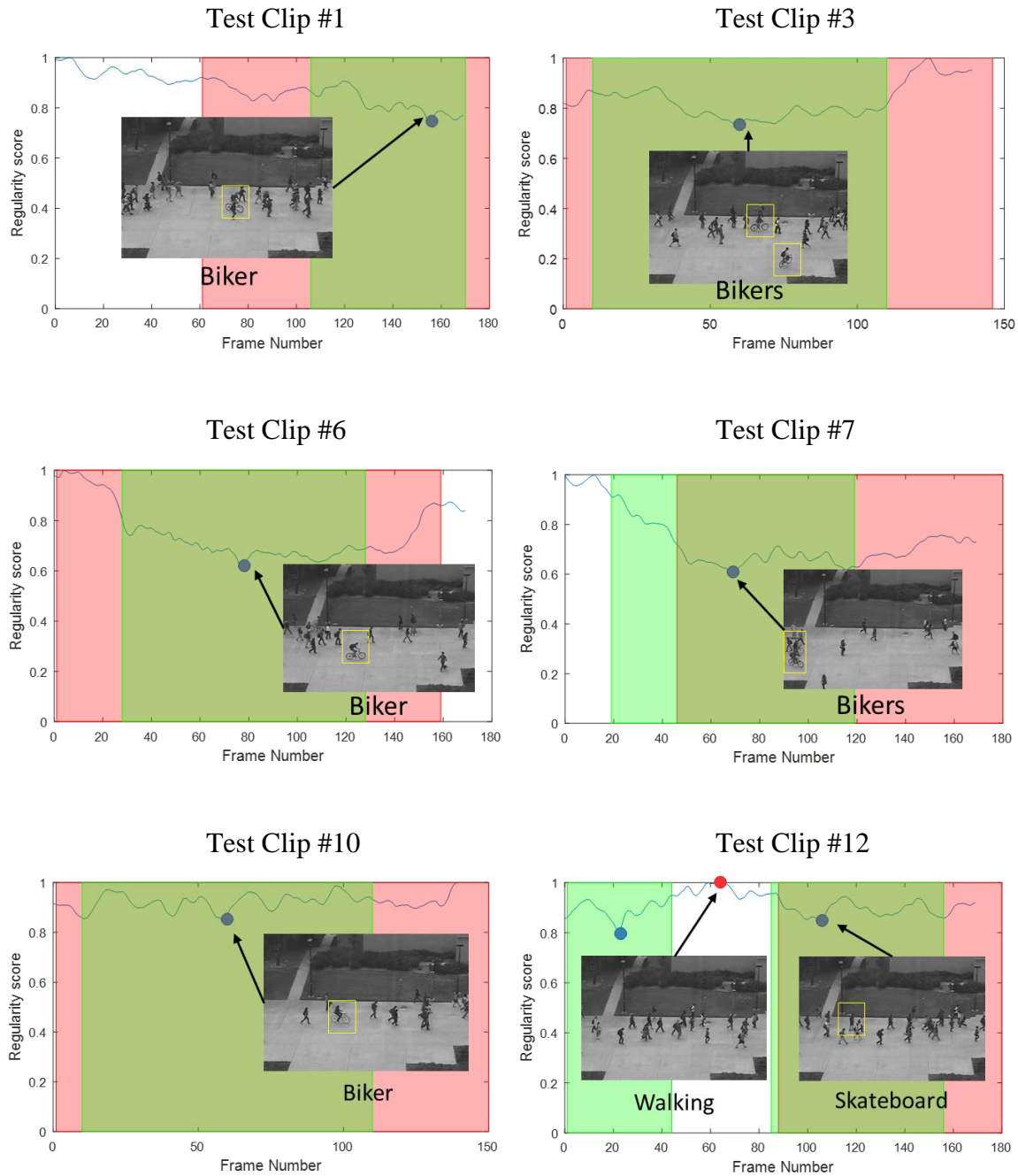


Figure 30: Anomaly evaluation graphs of test clips from the UCSD Pedestrian 1 dataset. Smaller areas of interest are highlighted with a yellow bounding box.

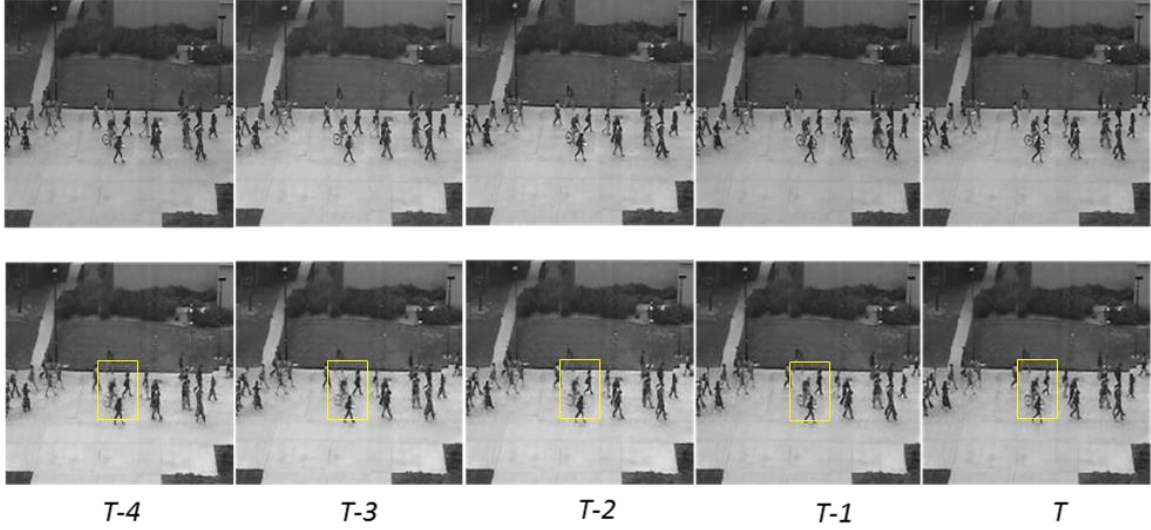


Figure 31: Input reconstruction obtained from the (224x224) Composite Conv-LSTM Encoder-Decoder Model on an *anomalous* sequence from test clip 1 of the UCSD Pedestrian 2 dataset. The first row is the input ground truth video sequences, while the second is the input reconstruction. Each column denotes a time-step. Regions of interest that change through time are highlighted by a yellow bounding box.

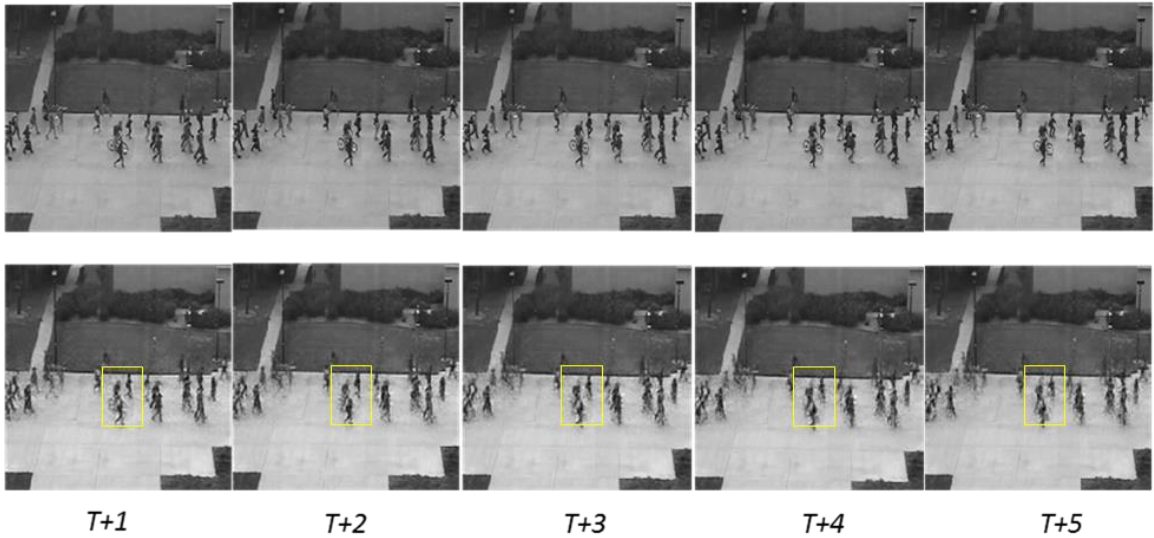


Figure 32: Future prediction obtained from the (224x224) Composite Conv-LSTM Encoder-Decoder Model on the *anomalous* sequence from test clip 1 of the UCSD Pedestrian 2 dataset used in Figure 32. The first row is the future ground truth video sequences, while the second is the output prediction. Each column denotes a time-step. Regions of interest that change through time are highlighted by a yellow bounding box

#### **4.4.3.2 Subway Entrance**

The subway entrance surveillance video contains a variety of anomalous activities that include commuters walking in the wrong direction, avoiding payment, and loitering. As there is only a single 1-hour long video, the first 15 minutes are used for training. A majority of the anomalies are detected with a 93.9% recall (Table 6). It should be noted that the last few seconds of the video are clipped off since the camera moves and it no longer pertains to the entrance. Unlike the UCSD Pedestrian dataset, the anomalous events in this dataset vary drastically in length. We leave the size of the temporal window denoting anomalous events at 100 frames so that it will be able to capture short events. While it does not report the entire anomalous segment for longer anomalous events, it is still able to detect the key moments in them to ensure that the event is found (Figure 33). A visualization of results from the model anomaly detection evaluation on four other clips from the Subway Entrance video can be found in Figure 34. A visualization of the model output is in Figures 35 and 36. The reconstruction and prediction of the person waiting on the station platform is clear and accurate. The figures of the two people walking across the camera, however, are significantly blurred with their positions in the prediction lagging behind the target ground truth. It should also be noted that the timestamp is not accurate as well because it constantly changed in the training data.

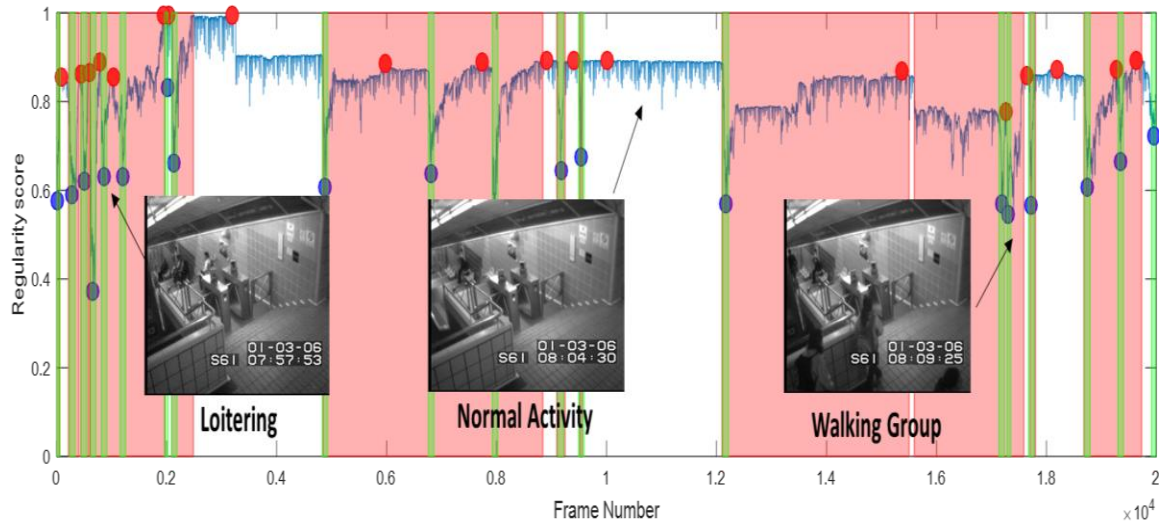


Figure 33: Regularity score (Eq.7) of frames 40,000–60,000 of the subway entrance. Distinct local minima are represented by a blue dot, distinct local maxima are represented by a red dot, the anomalous ground truth regions are highlighted in red, and the proposed anomalous regions are highlighted in green.

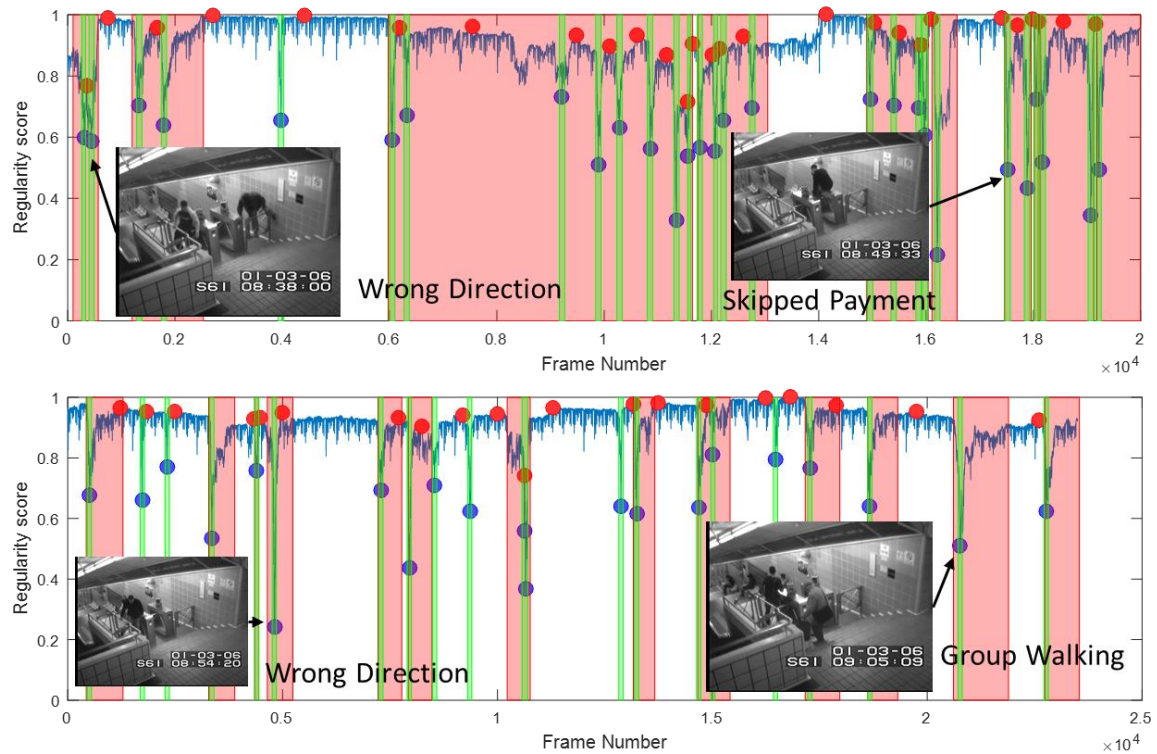


Figure 34: Regularity score (Eq.7) of frames 100,000-120,000 (top) and 120,000 – 144,000 (bottom) from the Subway Entrance video.

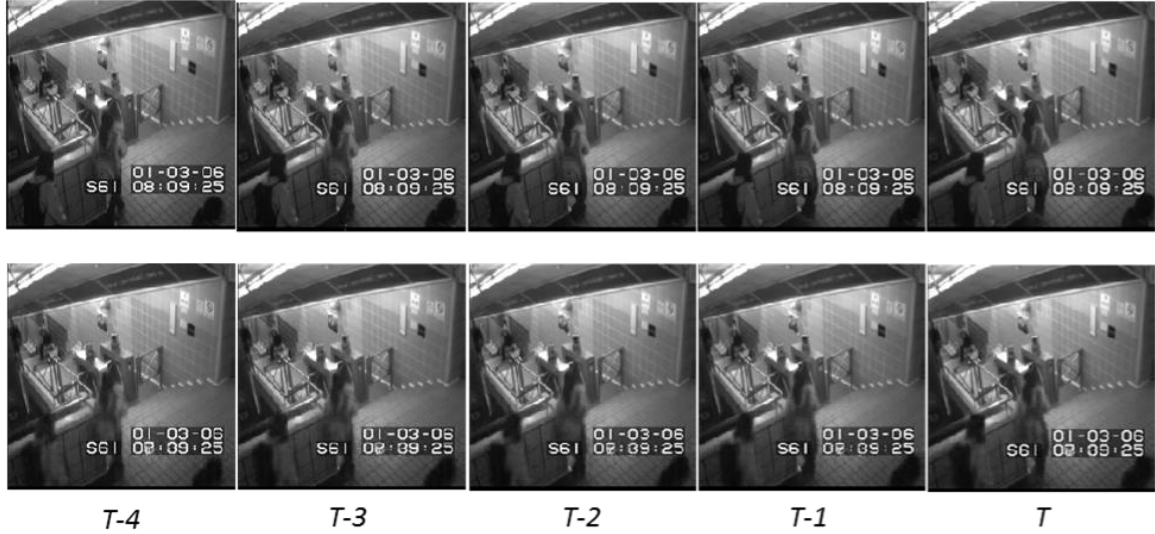


Figure 35: Input reconstruction obtained from the (224x224) Composite Conv-LSTM Encoder-Decoder Model on an *anomalous* sequence from the Subway Entrance video. The first row is the input ground truth video sequences, while the second is the input reconstruction. Each column denotes a time-step.

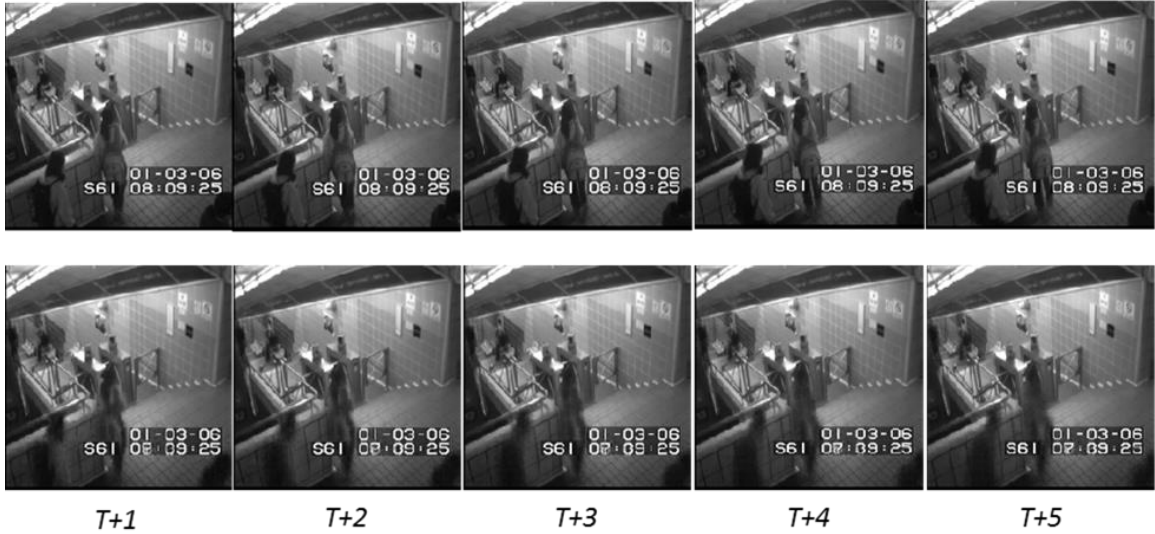


Figure 36: Future prediction obtained from the (224x224) Composite Conv-LSTM Encoder-Decoder Model on the *anomalous* sequence from the Subway Entrance video used in Figure 35. The first row is the future ground truth video sequences, while the second is the output prediction. Each column denotes a time-step.

#### 4.4.3.3 Subway Exit

The subway exit surveillance video contains a variety of anomalies similar to those found in the subway entrance video, and the first 15 minutes are used for training as well. Unlike the former video, the training data is not a good representation of usual events, with the majority of all action taking place at two short intervals and only one example of people exiting the station. Furthermore, there are several variations of normal events that occur in the testing data that are not present during training. This results in a skewed model that is unable to accurately model the regularity of a video. The issue is further amplified by the fact that the ground truth defines only nineteen anomalous events when there are in fact at least thirty. We do an evaluation using both the ground truth as provided from [4], and an updated one. As seen in Table 6, the model is able to detect every anomalous occurrence in both ground truth annotations. Since the training data does not provide an ample definition of what a regular event is, several of the regular events that take place in the video are falsely defined as irregular. Many of the false alarms, however, are actually regions in which an anomalous event takes place. When the trained model is evaluated using the updated ground truth annotation, performance improves significantly (Figure 37). The total number of anomalies detected decreases, as many of the previous false alarms fell under the same anomalous event, and each true anomalous event is only counted once. A visualization of results from the model anomaly detection evaluation on two other segments from the subway exit video can be found in Figure 38. A visualization of an anomalous model output is in Figures 39 and 40. Although the reconstruction and prediction of the moving group is not very accurate, it can be seen that the model fails to reconstruct or predict the single person in the group moving in the wrong direction.

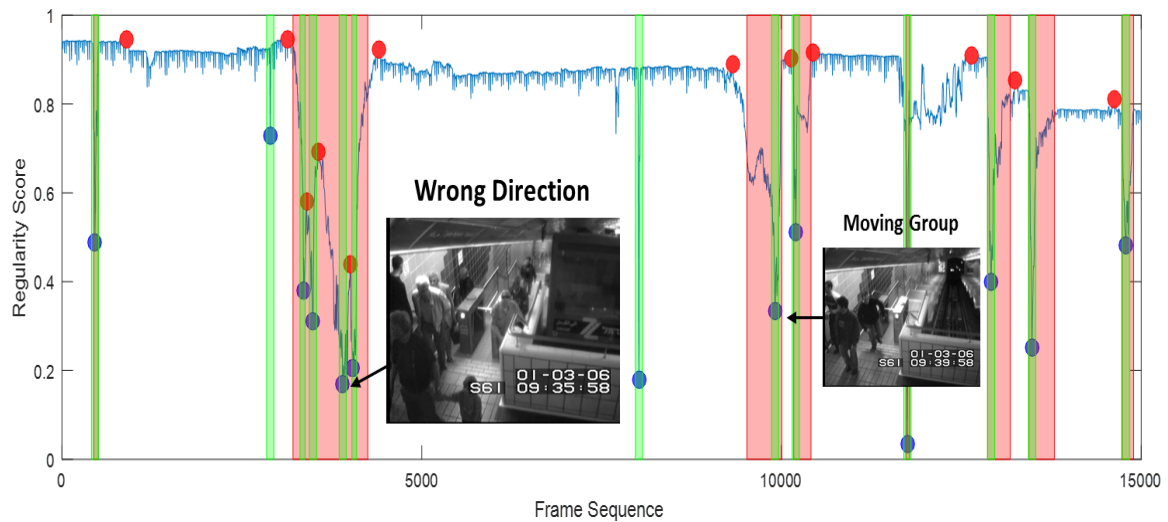


Figure 37: Regularity score (Eq.7) of frames 37,500–52,500 of the subway exit video.

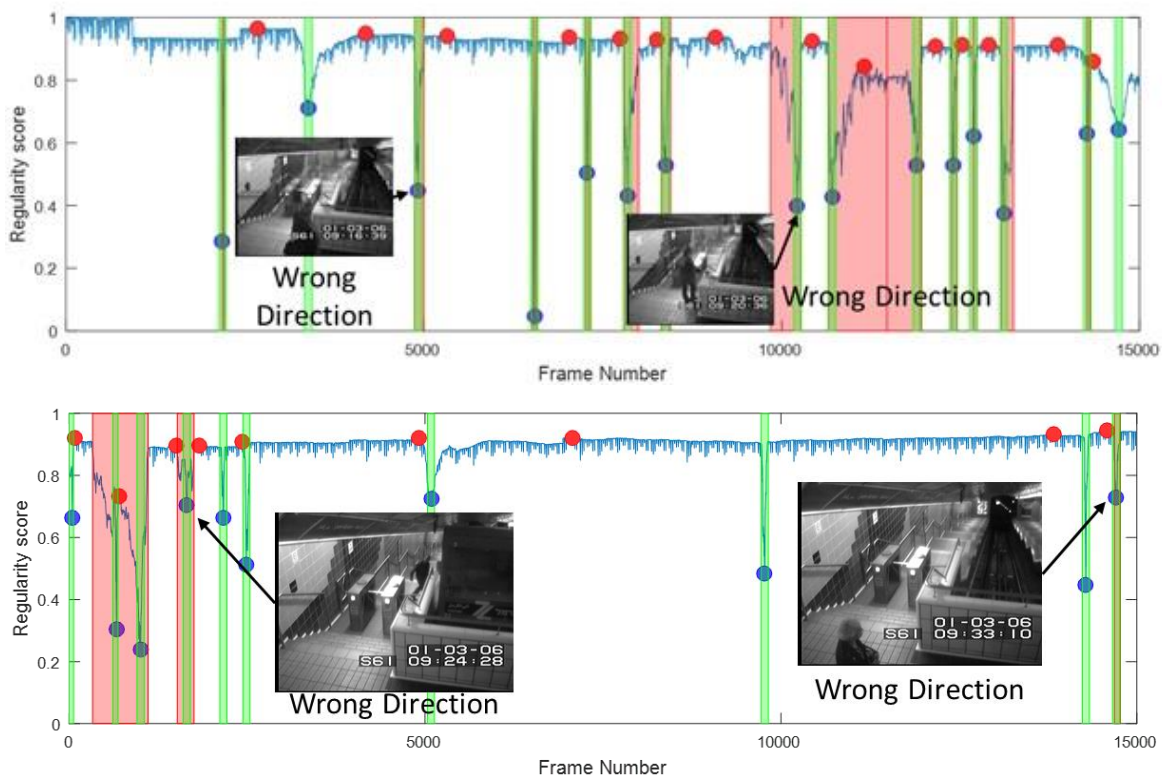


Figure 38: Regularity score (Eq.7) of frames 7,500–22,500 (top) and 22,500 – 37,500 (bottom) from the Subway Entrance video.

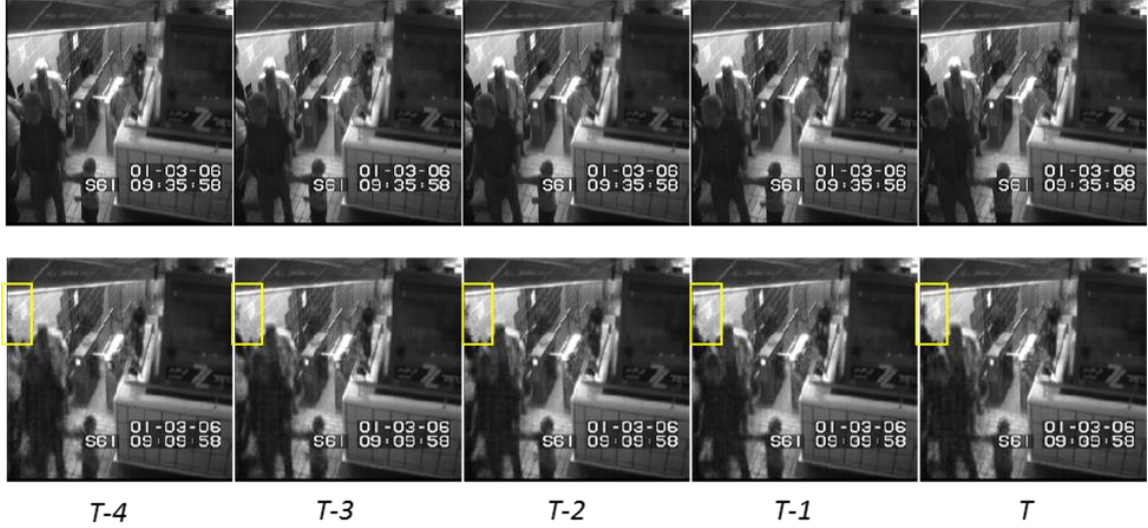


Figure 39: Input reconstruction obtained from the (224x224) Composite Conv-LSTM Encoder-Decoder Model on an *anomalous* sequence from the Subway Exit video. The first row is the input ground truth video sequences, while the second is the input reconstruction. Each column denotes a time-step. Regions of interest that change through time are highlighted by a yellow bounding box.

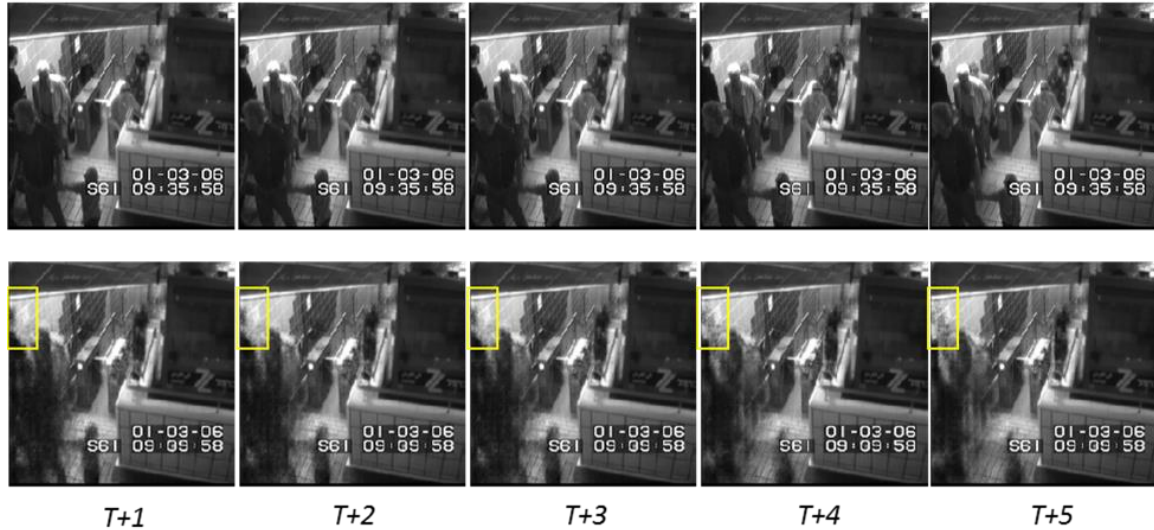


Figure 40: Future prediction obtained from the (224x224) Composite Conv-LSTM Encoder-Decoder Model on the *anomalous* sequence from the Subway Exit video used in Figure 39. The first row is the future ground truth video sequences, while the second is the output prediction. Each column denotes a time-step. Regions of interest that change through time are highlighted by a yellow bounding box.

#### **4.4.3.4 Avenue**

The Avenue dataset is split into training and testing data, with each video around 2 minutes long. The testing video clips contain a wide variety of anomalous events including but not limited to running, thrown objects, and walking in the wrong direction. The training video clips contain mostly “normal” activity, but do include a few irregular events. The proposed model is able to precisely differentiate between normal and anomalous activity in this dataset, but is unable to detect several anomalous events (Table 6) of the same type that occur in the background where most of the “normal” action takes place, and the pedestrians appear smaller. The anomalous event is of someone jogging. The evaluation algorithm is unable to differentiate the action of jogging from other pedestrians walking since the deviation in regularity caused by a smaller object in the background is much smaller than larger or more disruptive anomalous events (Figure 44). A visualization of results from the model anomaly detection evaluation on six other segments from the Avenue dataset can be found in Figure 43. A visualization of an anomalous model output for the dataset is in Figures 41 and 42. The figures of pedestrians walking in the background are seen to be clear in the reconstruction and only show a slight distortion in the prediction. The image of the woman walking directly in front of the camera shows significant deterioration. While her motion is modeled to some extent in the prediction, the spatial information for her figure is lost.

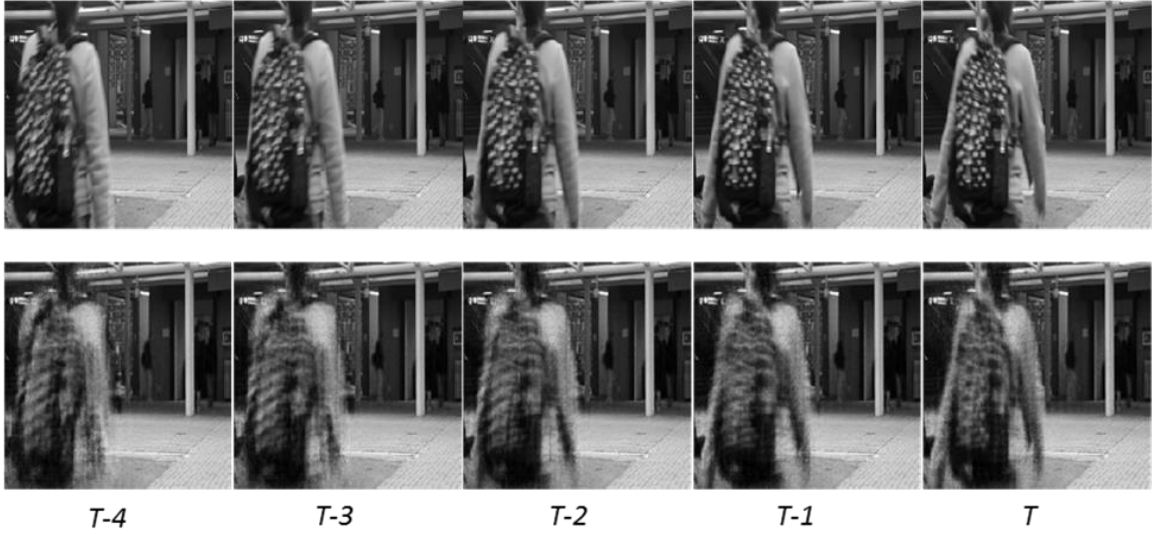


Figure 41: Input reconstruction obtained from the (224x224) Composite Conv-LSTM Encoder-Decoder Model on an *anomalous* sequence from test clip 1 of the Avenue dataset. The first row is the input ground truth video sequences, while the second is the input reconstruction. Each column denotes a time-step.

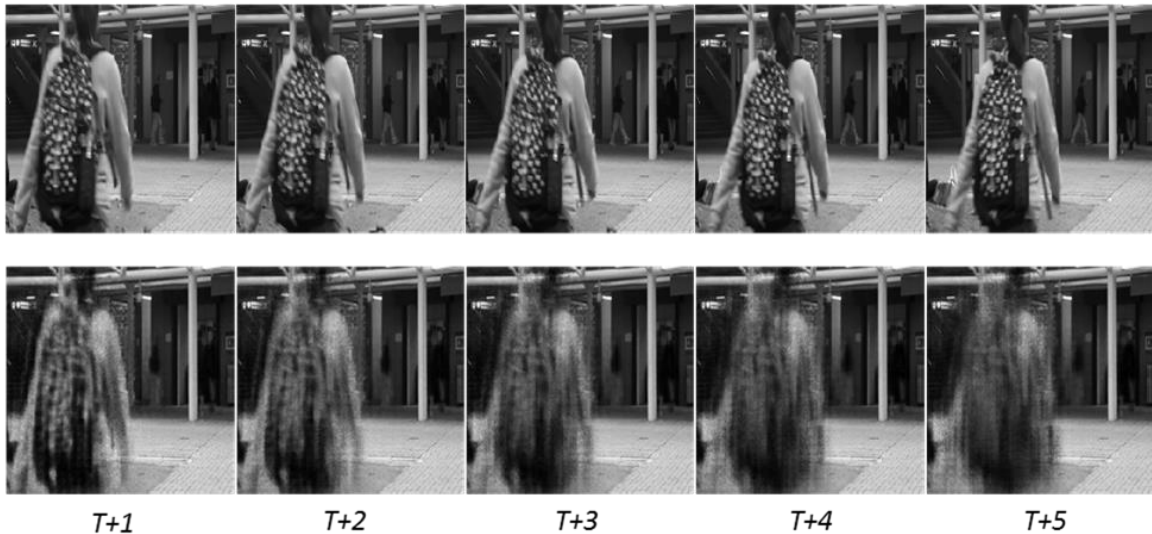


Figure 42: Future prediction obtained from the (224x224) Composite Conv-LSTM Encoder-Decoder Model on the *anomalous* sequence from the Avenue test clip used in Figure 41. The first row is the future ground truth video sequences, while the second is the output prediction. Each column denotes a time-step.

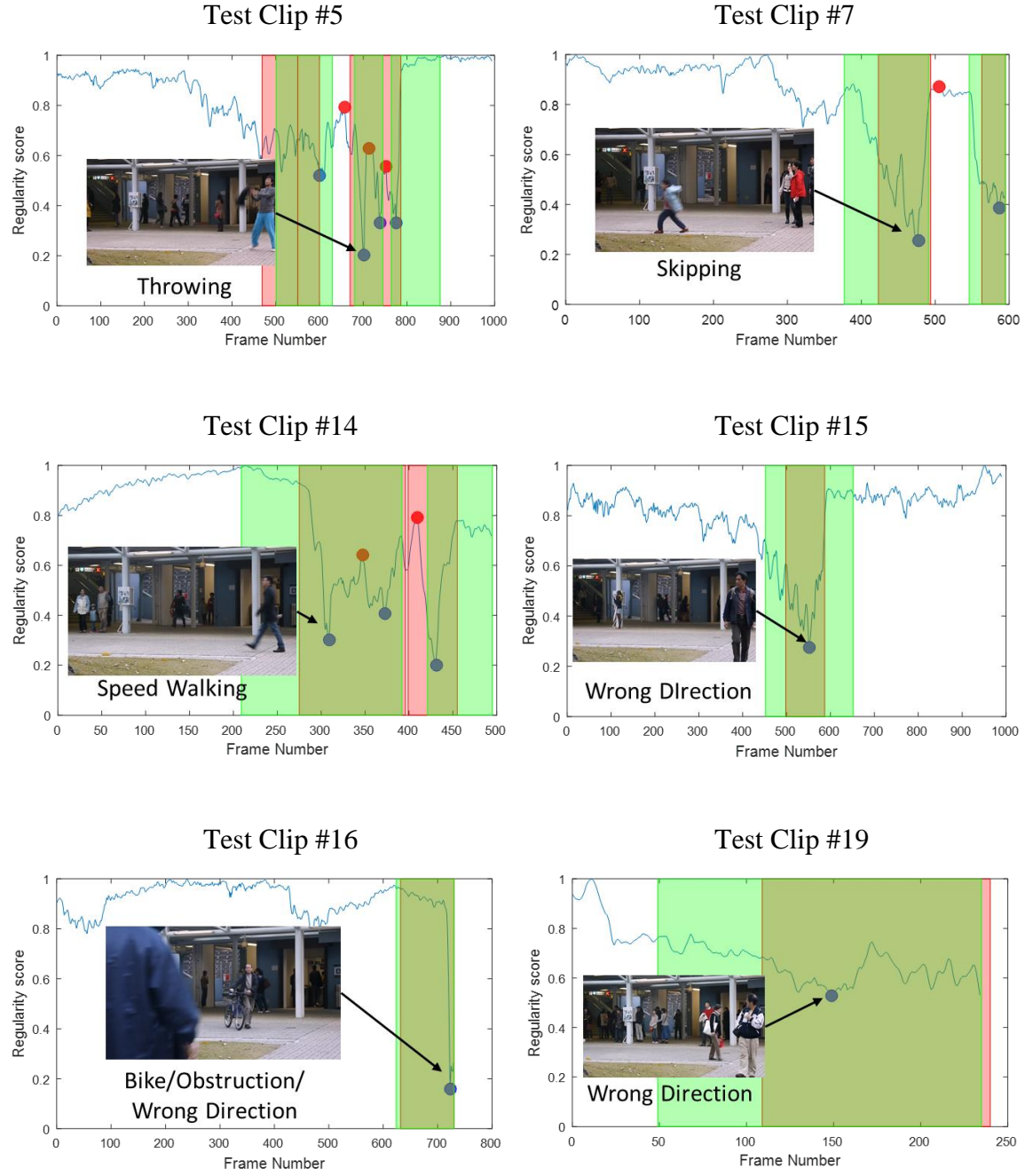


Figure 43: Anomaly evaluation graphs of test sequences from the Avenue dataset.

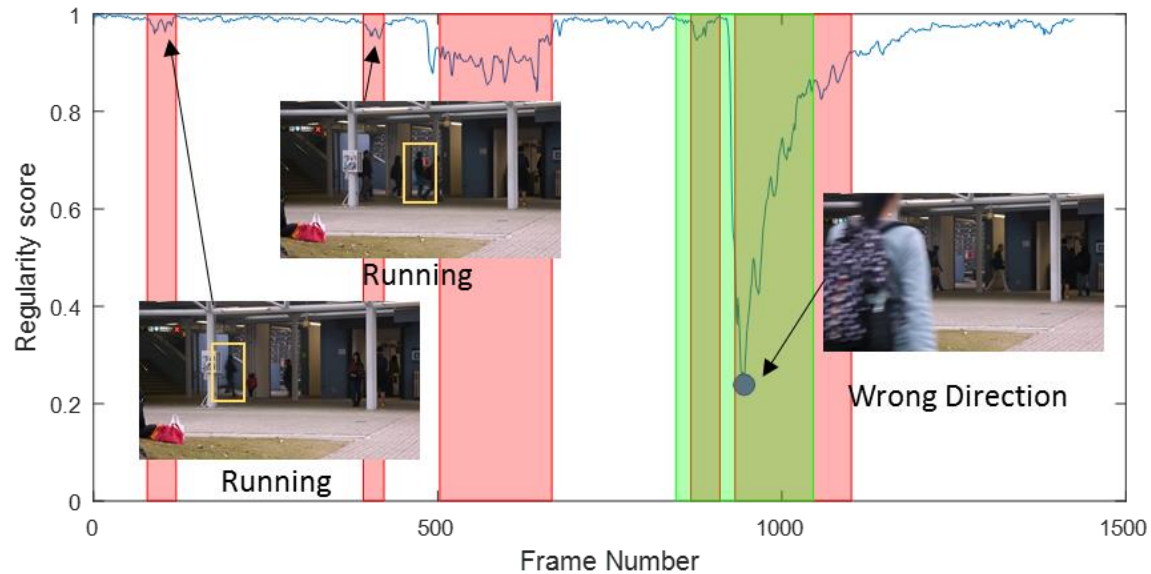


Figure 44: Regularity score (Eq.7) of test clip #1 of the Avenue dataset.

## Chapter 5 Conclusion

The aim of this thesis was to develop a network architecture able to model and predict video sequences for use in the detection of anomalies in related video segments.

The following contributions were presented in this work:

- Predictive Conv-LSTM networks able to accurately perform input reconstruction and predict subsequent video sequences.
- Development and investigation of composite and conditioned network structures
- Improved regularity evaluation for detecting anomalies in video sequences

The proposed composite Conv-LSTM network architecture is able to model video sequences, perform input reconstruction, and predict future frames. We apply the predictive capabilities of our network to determine anomalous events and locate points of interest in video sequences. A qualitative evaluation of the input reconstruction and future prediction of the proposed model demonstrates the predictive capabilities of Conv-LSTM units. A comparison of predictions between normal and anomalous events shows that our Conv-LSTM networks accurately model learned (familiar) movements but do not adapt to new (unusual) movements. This makes such networks effective for recognizing abnormalities when the training data is loosely supervised to contain mostly “normal” events. While the proposed model detects more false positives than previously proposed models, it also has an overall higher recall. A high recall is more important than precision when detecting anomalies, as it is better to find more than miss one altogether. Furthermore, the lower precision can generally be attributed to the lack of “normal” case samples within the datasets used. Given a loose supervision of training data to ensure that

most of it contains “normal” events, the networks are effective tools for recognizing abnormalities. A quantitative analysis shows that our method generally performs competitively to the state-of-the-art detection method, and performs better when sufficient information is given to the model during training. The proposed Conv-LSTM Encoder Decoder model has shown that convolutional LSTM units are effective enough at learning temporal features to predict subsequent video frames. Conv-LSTM units can therefore be applied to classification problems like action recognition that are dependent on spatio-temporal features.

## Bibliography

- [1] H. Zhong, J. Shi, and M. Visontai, “Detecting unusual activity in video,” in *CVPR*, 2004.
- [2] D. Zhang, D. Gatica-Perez, S. Bengio, and I. McCowan, “Semi-supervised adapted HMMs for unusual event detection,” in *CVPR*, 2005.
- [3] A. Adam, E. Rivlin, I. Shimshoni, and D. Reinitz, “Robust real-time unusual event detection using multiple fixed location monitors,” *Pattern Analysis and Machine Intelligence, IEEE Transactions on*, vol. 30, no. 3, pp. 555–560, 2008.
- [4] J. Kim and K. Grauman, “Observe locally, infer globally: a space-time mrf for detecting abnormal activities with incremental updates,” in *CVPR*, pp. 2921–2928, 2009.
- [5] L. Kratz and K. Nishino. “Anomaly detection in extremely crowded scenes using spatio-temporal motion pattern models,” in *CVPR*, pp. 1446–1453, 2009.
- [6] Y. Benezeth, P. Jodoin, V. Saligrama, and C. Rosenberger. “Abnormal events detection based on spatio-temporal occurrences,” in *CVPR*, 2009.
- [7] R. Mehran, A. Oyama, and M. Shah. “Abnormal crowd behavior detection using social force model,” in *CVPR*, pp. 935–942, 2009.
- [8] V. Mahadevan, W. Li, V. Bhalodia, and N. Vasconcelos, “Anomaly detection in crowded scenes,” in *CVPR* pp. 1975–1981, 2010.
- [9] B. Zhao, L. Fei-Fei, and E. P. Xing, “Online detection of unusual events in videos via dynamic sparse coding,” in *CVPR* pp. 3313–3320, 2011.
- [10] Y. Cong, J. Yuan, and J. Liu, “Sparse Reconstruction Cost for Abnormal Event Detection,” in *CVPR*, pp. 3449–3456, 2011.
- [11] X. Cui, Q. Liu, M. Gao, and D. Metaxas. “Abnormal detection using interaction energy potentials,” in *CVPR*, pp. 3161–3167, 2011.
- [12] F. Jiang, J. Yuan, S. A. Tsaftaris, and A. K. Katsaggelos, “Anomalous video event detection using spatiotemporal context,” in *Computer Vision and Image Understanding*, 115(3), pp. 323–333, 2011.
- [13] V. Saligrama and Z. Chen, “Video anomaly detection based on local statistical aggregates,” in *CVPR*, pp. 2112–2119, 2012.
- [14] C. Lu, J. Shi, and J. Jia, “Abnormal event detection at 150 fps in Matlab,” in *ICCV*, pp. 2720–2727, 2013.
- [15] M. Hasan, J. Choi, J. Neumann, A. Roy-Chowdhury, L. Davis, “Learning Temporal Regularity in Video Sequences,” in *CVPR*, 2016.
- [16] Chandola, Varun, Arindam Banerjee, and Vipin Kumar. "Anomaly detection: A survey." *ACM computing surveys (CSUR)* 41.3 (2009): 15.

- [17] Shi, Xingjian, Chen, Zhourong, Wang, Hao, Yeung, Dit-Yan, Wong, Wai-Kin, and Woo, Wangchun. Convolutional LSTM network: A machine learning approach for precipitation nowcasting. CoRR, abs/1506.04214, 2015
- [18] Patraucean, Viorica, Ankur Handa, and Roberto Cipolla. "Spatio-temporal video autoencoder with differentiable memory." arXiv preprint arXiv:1511.06309 (2015).
- [19] N. Srivastava, E. Mansimov, and R. Salakhutdinov. Unsupervised learning of video representations using lstms. In ICML, 2015
- [20] Ballas, Nicolas, et al. "Delving Deeper into Convolutional Networks for Learning Video Representations." arXiv preprint arXiv:1511.06432 (2015).
- [21] Bishop, Christopher M.: Pattern Recognition and Machine Learning. Springer. 2007.
- [22] LeCun, Yann, et al. "Gradient-based learning applied to document recognition." *Proceedings of the IEEE* 86.11 (1998): 2278-2324.
- [23] J. L. Elman. Finding structure in time. *Cognitive Science*, 14:179–211, 1990.
- [24] Mike Schuster and Kuldip K. Paliwal, *Bidirectional Recurrent Neural Networks*, Trans. on Signal Processing 1997
- [25] Alex Graves, Santiago Fernandez, and Jurgen Schmidhuber, *Multi-Dimensional Recurrent Neural Networks*, ICANN 2007
- [26] S. Hochreiter and J. Schmidhuber. Long Short-Term Memory. *Neural Computation*, 9(8):1735–1780, 1997
- [27] Graves, Alex. "Generating sequences with recurrent neural networks." arXiv preprint arXiv:1308.0850 (2013).
- [28] Khurram Soomro, Amir Roshan Zamir and Mubarak Shah, UCF101: A Dataset of 101 Human Action Classes From Videos in The Wild, CRCV-TR-12-01, November, 2012.
- [29] LeCun, Yann, Corinna Cortes, and Christopher JC Burges. "The MNIST database of handwritten digits." (1998).
- [30] Y. Kozlov and T. Weinkauf, “Persistence1D: Extracting and filtering minima and maxima of 1d functions,” <http://people.mpi-inf.mpg.de/~weinkauf/notes/persistence1d.html>, accessed: 2016-09-02.

- [31] T. Tieleman and G. Hinton. Lecture 6.5 - RMSProp: Divide the gradient by a running average of its recent magnitude. Coursera Course: Neural Networks for Machine Learning, 4, 2012
- [32] F. Rosenblatt, "The perceptron: A probabilistic model for information storage and retrieval in the brain," In Neurocomputing: foundations of research, 1st ed. MIT Press Cambridge, MA 1988 pp. 89-114
- [33] J. Duchi, E. Hazan, and Y. Singer, "Adaptive subgradient methods for online learning and stochastic optimization," The Journal of Machine Learning Research, vol. 12, pp. 2121–2159, 2011. 5
- [34] D. Kingma and J. Ba, "Adam: A Method for Stochastic Optimization," arXiv:1412.6980, 2015. 5
  
- [35] Glorot and Y. Bengio, "Understanding the difficulty of training deep feedforward neural networks," in AISTAT, 2010. 5
  
- [36] Khurram Soomro, Amir Roshan Zamir and Mubarak Shah, [UCF101: A Dataset of 101 Human Action Classes From Videos in The Wild](#), CRCV-TR-12-01, November, 2012
  
- [37] Bengio, Ian Goodfellow Yoshua, and Aaron Courville. "Deep learning. Book in preparation for MIT Press." URL <http://www.deeplearningbook.org> (2016).
  
- [38] Sutskever, Ilya, James Martens, and Geoffrey E. Hinton. "Generating text with recurrent neural networks." *Proceedings of the 28th International Conference on Machine Learning (ICML-11)*. 2011.
  
- [39] Malinowski, Aleksander, Tomasz J. Cholewo, and Jacek M. Zurada. "Capabilities and Limitations of Feedforward Neural Networks with Multilevel Neurons." *ISCAS*. 1995.